

Bone histology and growth curve of the earliest ceratopsian *Yinlong downsi* from the Upper Jurassic of Junggar Basin, Northwest China

Fenglu Han¹, Qi Zhao², Jinfeng Hu¹ and Xing Xu^{2,3}

¹ School of Earth Sciences, China University of Geosciences (Wuhan), Wuhan, China

² Key Laboratory of Vertebrate Evolution and Human Origins, Institute of Vertebrate Paleontology and Paleoanthropology, Chinese Academy of Sciences, Beijing, China

³ Centre for Vertebrate Evolutionary Biology, Yunnan University, Kunming, China

ABSTRACT

Yinlong downsi, the earliest known ceratopsian, is represented by dozens of specimens of different sizes collected from the Upper Jurassic of the Junggar Basin, northwestern China. Here, we present the first comprehensive study on the bone histology of *Yinlong downsi* based on ten specimens varying in size. Four ontogenetic stages are recognized: early juvenile, late juvenile, subadult, and adult. The reconstructed growth curve suggests that *Yinlong* may reach sexual maturity at 6 years old, which is earlier than that of the well-studied early-diverging ceratopsian *Psittacosaurus* (9 years old) but later than ceratopsids (about 3 to 5 years old). This may indicate that sexual maturity begins earlier during the evolution of ceratopsians, and that the giant size of ceratopsids is acquired by accelerating growth rates. The cortex of the tibia mainly consists of fibrolamellar bone tissues, but parallel-fibered bone and lines of arrested growth (LAGs) are very common throughout ontogeny, suggesting a moderate growth rate. Quantitative analysis indicates that *Yinlong* has a maximum growth rate similar to those of other small-sized dinosaurs such as *Psittacosaurus*, *Dysalotosaurus*, and *Troodon*, and their maximum growth rates are higher than those of extant squamates and crocodiles but lower than those of extant mammals and large dinosaurs. This suggests that body size plays a more important role in growth rate than other factors such as phylogenetic position and/or diet among non-avian dinosaurs.

Submitted 14 August 2024
Accepted 4 December 2024
Published 19 December 2024

Corresponding author
Fenglu Han, hanfl@cug.edu.cn

Academic editor
Blanca Moncunill-Solé

Additional Information and
Declarations can be found on
page 22

DOI 10.7717/peerj.18761

© Copyright
2024 Han et al.

Distributed under
Creative Commons CC-BY 4.0

OPEN ACCESS

Subjects Evolutionary Studies, Paleontology, Zoology, Histology

Keywords Bone histology, Dinosaur, Ceratopsia, Jurassic, Junggar Basin, China, *Yinlong*, Growth curve

INTRODUCTION

Ceratopsia is a successful, large group of herbivorous non-avian dinosaurs that lived from the Late Jurassic to the end of the Cretaceous (*You & Dodson, 2004*). The early-diverging ceratopsians are all bipedal dinosaurs. They have rostral bones, relatively large skulls without horns, and relatively small body sizes, such as *Yinlong*, *Psittacosaurus*, *Liaoceratops*, *Archaeoceratops*, and *Auroraceratops* (*Dong & Azuma, 1997; Xu et al., 2002; You & Dodson, 2004; You et al., 2005; Xu et al., 2006*). Most of these materials are well

studied in morphology and phylogeny (You & Dodson, 2003; Han et al., 2018; Morschhauser et al., 2018a, 2018c), but the ontogenetic variation of bone microstructure in early-diverging ceratopsians is still rarely known, except in *Psittacosaurus*. This latter species shows fibrolamellar bone with lines of arrested growth (LAGs) and was supposed to have faster growth rates than extant reptiles (Erickson & Tumanova, 2000; Erickson et al., 2009; Zhao et al., 2019; Skutschas et al., 2021). In addition, histological data support an ontogenetic shift from quadrupedality to bipedality (Zhao et al., 2013), and also suggest social behavior among different ages (Hedrick et al., 2014; Zhao et al., 2014).

Ontogenetic changes in bone microstructure of ceratopsians were also studied in *Protoceratops*, *Cerasinops*, *Koreaceratops*, the ceratopsids *Einosaurus*, *Pachyrhinosaurus*, *Centrosaurus*, *Avaceratops*, *Yuehecauhceratops*, *Utahceratops*, *Kosmoceratops* and *Triceratops* (Chinnery & Horner, 2007; Reizner, 2010; Erickson & Druckenmiller, 2011; Horner & Lamm, 2011; Levitt, 2013; Fostowicz-Frelik & Słowiak, 2018; Hedrick et al., 2020; Baag & Lee, 2022; de Rooij et al., 2024). The Late Cretaceous *Protoceratops* is a small quadrupedal ceratopsian and possibly exhibits social behavior, as suggested for *Psittacosaurus* (Fastovsky et al., 2011). *Protoceratops* has a similar vascular pattern to *Psittacosaurus* but with no apparent LAGs and more fossilized fibers to strengthen the tissue (Fostowicz-Frelik & Słowiak, 2018). Bone microstructure of the non-coronosaurian neoceratopsians *Koreaceratops* is more similar to that of *Protoceratops* than to *Psittacosaurus* in preserving zonation of the tibia and LAGs in the fibula (Baag & Lee, 2022).

The large-sized ceratopsids are composed of fibrolamellar bone as in other ceratopsians, but the bone microstructure of centrosaurines and chasmosaurines is possibly different. The former is more like non-ceratopsid ceratopsians by preserving LAGs and lacks bone remodeling throughout the whole cortex, whereas the latter has few LAGs and strong bone remodeling throughout the cortex (Levitt, 2013; Hedrick et al., 2020; de Rooij et al., 2024). The centrosaurine *Einosaurus* reaches its highest growth rate between 3 and 5 years, which is earlier than that of *Psittacosaurus* (Reizner, 2010). The humeri of *Triceratops* display a mix of longitudinal and circumferential vascular canals and bone remodeling happens in a very early stage, but LAGs appear very late (de Rooij et al., 2024).

Yinlong downsi is the earliest known ceratopsian recorded globally from the Upper Jurassic Shishugou Formation of Junggar Basin, China (Xu et al., 2006). It has a small body size (about 1–2 m in length) with a relatively large skull as in *Psittacosaurus*. *Yinlong* provides key features for understanding the evolution of early ornithischians, supporting the monophyly of Marginocephalia and its close relationship to Heterodontosauridae, although the latter is recovered as the most basal ornithischians in most phylogenetic analyses (Xu et al., 2006; Butler, Upchurch & Norman, 2008; Fonseca et al., 2024). Recent phylogenetic analyses support *Yinlong* to be within Chaoyangosauridae, which forms a monophyly with either *Psittacosaurus* or Neoceratopsia (Han et al., 2018; Morschhauser et al., 2018b; Yu et al., 2020). Abundant materials have been discovered allowing for a detailed study of skeletal morphology (Han et al., 2016, 2018), ontogeny, and dental system

([Hu et al., 2022](#)). However, there is still no detailed study on the growth pattern of *Yinlong* based on bone histology, hindering our understanding of the evolution of physiology and behavior in early ceratopsians and ornithischians. Here we provide an in-depth investigation to study ontogenetic variation and growth curvature and compare it with other ceratopsians and early diverging ornithischians, elaborating on the variation of growth patterns during the evolution of ceratopsians. In addition, bone microstructure from early ornithischians (Triassic and Jurassic) is relatively rarely known, and only a few taxa, such as *Lesothosaurus* ([Knoll, Padian & de Ricqlès, 2010](#)), heterodontosaurid remains ([Becerra et al., 2016](#)), have been primarily studied. The detailed ontogenetic study of bone histology in *Yinlong* will provide important evidence for understanding the evolution of physiology and behavior in early ornithischians.

MATERIALS AND METHODS

Material

Ten individuals of *Yinlong downsi* were selected for histological analysis ([Table 1](#)). All the materials come from the Upper Jurassic Shishugou Formation of the Wucuiwan area, Xinjiang, China ([Han et al., 2016, 2018](#)). Identification of these materials is accurate if they have skulls, as *Yinlong* preserved many autapomorphies on its skull ([Xu et al., 2006; Han et al., 2016](#)). However, caution should be exercised if there are only postcranial bones, as they are quite similar to those of the small ornithopod *Gongbusaurus wucuiwanensis* ([Dong, 1989](#)) and another ceratopsian *Hualianceratops wucuiwanensis* ([Han et al., 2015](#)). Among these sampled ten individuals, eight have complete or partial skulls associated with postcranial elements, and only the two specimens IVPP V18677 and IVPP V18682 solely preserved the postcranial elements, but they have been well described in detail as *Yinlong* by [Han et al. \(2018\)](#). According to our observations, *Yinlong* differs from *Gongbusaurus* by its relatively robust femur, elongated ilium, blade-like prepubic process, and short postpubic shaft. *Hualianceratops* was another ceratopsian from the same stratigraphic layer as *Yinlong* ([Han et al., 2015](#)). *Hualianceratops* differs from *Yinlong* by its skull elements, but they have no differences in the postcranial materials. *Hualianceratops* was established only by one specimen, whereas *Yinlong* was represented by dozens of individuals. Here the preserved postcranial elements of IVPP V18677 and IVPP V18682 were possibly *Yinlong*, but *Hualianceratops* could not be excluded entirely.

All the materials were photographed and measured before sectioning. The preparation of most of these sections (IVPP V18677, IVPP V18678, IVPP V18636, IVPP V18679, IVPP V18682, IVPP V18683, IVPP V18637) was performed in the IVPP (Institute of Vertebrate Paleontology and Paleoanthropology). These samples were processed using the Exakt-Cutting-Grinding System ([Donath & Rohrer, 2003](#)), and the detailed method was provided in [Han et al. \(2020\)](#). The other sections (IVPP V33266, IVPP V33267, IVPP V33268) were prepared at the fossil lab, School of Earth Sciences, China University of Geosciences (Wuhan) ([Ke et al., 2021](#)). Sections were sampled mainly from the mid-diaphyses of the tibia, fibula, and ribs ([Table 1; Fig. S1](#)). The sectional sides were photographed using a Zeiss Primotech microscope. Throughout the text, bone histological terminology and definitions follow [Francillon-Viellet et al. \(1990\)](#) and [Chinsamy-Turan \(2005\)](#).

Table 1 Basic dataset of sectional bones used for the calculation of growth curves.

| Specimen number | Sectional bones | Femur circumferences (cm) | Femur length | Tibia length | Fibula length | Visible LAGs | Total LAGs | Body mass 1 (kg) | Body mass 2 (kg) |
|-----------------|-----------------|---------------------------|--------------|--------------|---------------|--------------|------------|------------------|------------------|
| IVPP V18677 | Tibia | 50 | 135 | 164 | 160 | 2 (1) | 3 | 9 | 12 |
| | Fibula | | | | | 3 (0) | 3 | | |
| IVPP V33266 | Tibia | 74 | 155 (E) | 180 | 174 | 4 (1) | 5 | 20 | 28 |
| | Fibula | | | | | 5 | 5 | | |
| IVPP V18678 | Tibia | 70 | 150 (E) | ? | ? | 4 (1) | 5 | 17 | 24 |
| IVPP V33267 | Tibia | ? | ? | 172 | >147 | 5 | 5 | ? | ? |
| IVPP V18636 | Tibia | 86 | 178 | ? | ? | 4 (3) | 7 | 31 | 42 |
| | Fibula | | | | | 5 (2) | 7 | | |
| | Rib | | | | | 7 (0) | 7 | | |
| IVPP V18679 | Tibia | 90 | >170 | >121 | ? | 5 (2) | 7 | 35 | 48 |
| | Fibula | | | | | ? | ? | | |
| | Rib | | | | | 4 (3) | 7 | | |
| IVPP V18682 | Fibula | ? | 177 | 196 | >175 | 6 (2) | 8 | ? | ? |
| | Rib | | | | | 6 (2) | 8 | | |
| IVPP V18683 | Tibia | 97 | 189 | 210 | 198 | 8 (4) | 12 | ? | ? |
| | Fibula | | | | | 9 (2) | 11 | | |
| | Rib | | | | | 10 (1) | 11 | | |
| IVPP V33268 | Fibula | 100 | >164 | 214 | >167 | ? | ? | 46 | 64 |
| IVPP V18637 | Tibia | 100 | ? | 201 | | 11 (2) | 13 | 46 | 64 |

Note:

“E” denotes estimated values. The numbers in parentheses denote the estimated erosion LAGs. Body mass 1 and 2 correspond to the studies by *Anderson, Hall-Martin & Russell (1985)* and *Campione et al. (2014)*, respectively.

Body mass estimation

The body mass of bipedal dinosaurs is usually estimated by the following two equations:

$$\text{Mass}_{\text{biped}} = 0.16 \text{FC}^{2.73} \text{ (Anderson, Hall-Martin \& Russell, 1985).}$$

$$\text{Mass}_{\text{biped}} = (10^{(2.749 * \log_{10}(\text{FC} * 2^{0.5}) - 1.104)}) / 1,000 \text{ (Campione et al., 2014; Benson et al., 2018).}$$

FC indicates the minimum circumference of a femur, which has been acquired in seven individuals (Table 1).

Longevity and growth rate calculation

Estimation of individual age was calculated by counting LAGs in tibiae, fibulae, and ribs (Fig. 1). We preferred to count the LAGs in the ribs for relatively small individuals (IVPP V33266, IVPP V18636), which usually preserved the most complete LAGs because of a small medullary cavity and less remodeled than the fibulae and tibiae (*Waskow & Sander, 2014; Fostowicz-Frelik & Słowiak, 2018; Hedrick et al., 2020; de Rooij et al., 2024*).

Therefore, longevity could be directly estimated by preserving LAGs in small individuals. However, in large individuals, inner bone erosion happened in all sectional bones, and longevity was estimated referring to the estimated LAGs of the tibia, fibula, and ribs.

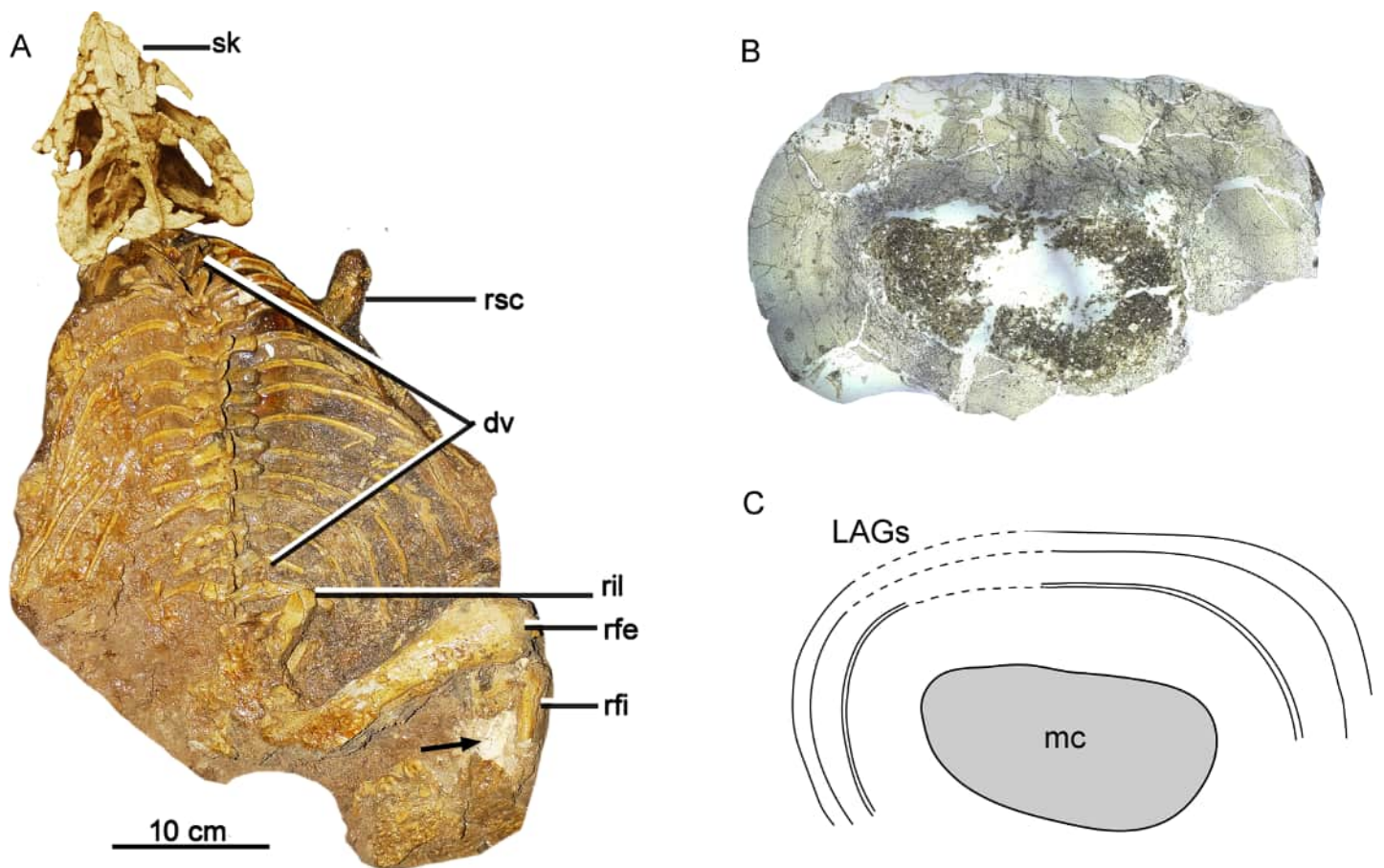


Figure 1 Skeleton and bone microstructure of the subadult individual IVPP V18636. (A) Skull and postcranial skeleton in dorsal view. The black arrow denotes the sampled position. Cross-section (B) and line drawing LAGs (C) of the right tibia. Abbreviations: dv, dorsal vertebrae; mc, medullary cavity; rfe, right femur; rfi, right fibula; ril, right ilium; rsc, right scapula; sk, skull. [Full-size !\[\]\(b345a1c4255362eec3746050dd71ccac_img.jpg\) DOI: 10.7717/peerj.18761/fig-1](https://doi.org/10.7717/peerj.18761/fig-1)

Missing LAGs destroyed by the expansion of the medullary cavity are recalculated by using the extrapolation method (Klein & Sander, 2007). The distance between the center of medullary cavity and the first visible LAG was divided by the greatest distance between any two adjacent LAGs. The result of the calculation is the maximal number of estimated LAGs as the resorbed cycle is wider than any preserved ones (Table 1; Fig. S2). Therefore, it is more accurate to subtract one. The total estimated LAG was calculated using the following equation:

$$N_{\text{est}} = N_{\text{pre}} + (D_{\text{cf}}/D_{\text{max}}) - 1$$

N_{est} denotes the total estimated LAGs. N_{pre} denotes preserved LAGs. D_{cf} means the distance between the center of the medullary cavity to the first LAGs. D_{max} means the greatest distance between the preserved adjacent LAGs.

Growth rate estimation of consecutive years was obtained by subtracting body mass values. To compare with the maximal growth rates of extant animals, the rates were then converted to daily values by dividing each by 379 days in 1 year of the Late Jurassic (Wells,

1963). The converted daily data value was compared to the data of extant vertebrate taxa of similar size (Erickson, Rogers & Yerby, 2001; Hübner, 2012).

Growth curves

Here we established the growth curves according to Erickson & Tumanova (2000). The estimated body mass was plotted against their age in years. Establishing the growth curves was analyzed using the statistical software Origin 8.0. The equation $\text{mass} = a/(1 + \exp(b(\text{Age} + c)))$ was chosen to describe the sigmoidal growth curve (a, largest known body mass; b, c denote parameters to fit). As mentioned above, we used two methods to estimate the body mass and got two growth curves. The body mass estimation by Anderson, Hall-Martin & Russell (1985) was mainly based on extant mammals ratites, whereas Campione et al. (2014) analyzed more birds and got significantly lower errors. However, the formula of Anderson, Hall-Martin & Russell (1985) is commonly used for estimating the body mass of non-avian dinosaurs before the publication of Campione et al. (2014) and there is more data on the growth curve based on the former. Here we used both of these methods for body mass estimation to establish growth curves.

To compare the maximum growth rate of *Yinlong* with other dinosaurs and extant animals, we used the dataset of Grady et al. (2014). The regression of adult body mass and maximum growth rates of crocodylians, placental mammals, marsupials, altricial birds, precocial birds, squamates, and dinosaurs were calculated and used for comparison. The body mass estimation of *Yinlong* was based on Anderson, Hall-Martin & Russell (1985) for consistency with other dinosaurs.

RESULTS

The bone histology of *Yinlong downsi* consists of fibrolamellar bone tissue with high cortical porosity, but the parallel fibered bone tissue and LAGs are common throughout ontogeny, suggesting that *Yinlong* has a moderate growth rate. Here, we divided the growth of *Yinlong* into four stages, including early juvenile, late juvenile, subadult, and adult, based on a combination of features of bone microstructure. The description of each stage is mainly based on the tibia. Fibulae and ribs are also described for comparison.

Early juvenile stage

IVPP V18677 is the smallest individual, with a femur length of approximately 135 mm (Table 1). The bone microstructure of the tibia and fibula was examined and corresponds to the early juvenile stage (Fig. 2). The sampled partial cortex of the tibia is highly vascularized, with most vascular canals oriented longitudinally and only a few anastomosing canals present (Fig. 2C). Primary osteons are well developed throughout the cortex, while secondary osteons are absent at this stage. Two indistinct LAGs are present, dividing the cortex into three circumferential regions (Fig. 2A). Under polarized light, the cortex mainly consists of fibrolamellar bone, but parallel-fibered bone tissue is prevalent throughout the cortex, and increases in density towards the LAG and the bone surface (Figs. 2B, 2D), suggesting alternating rapid and slow growth rates. Notably, both the inner

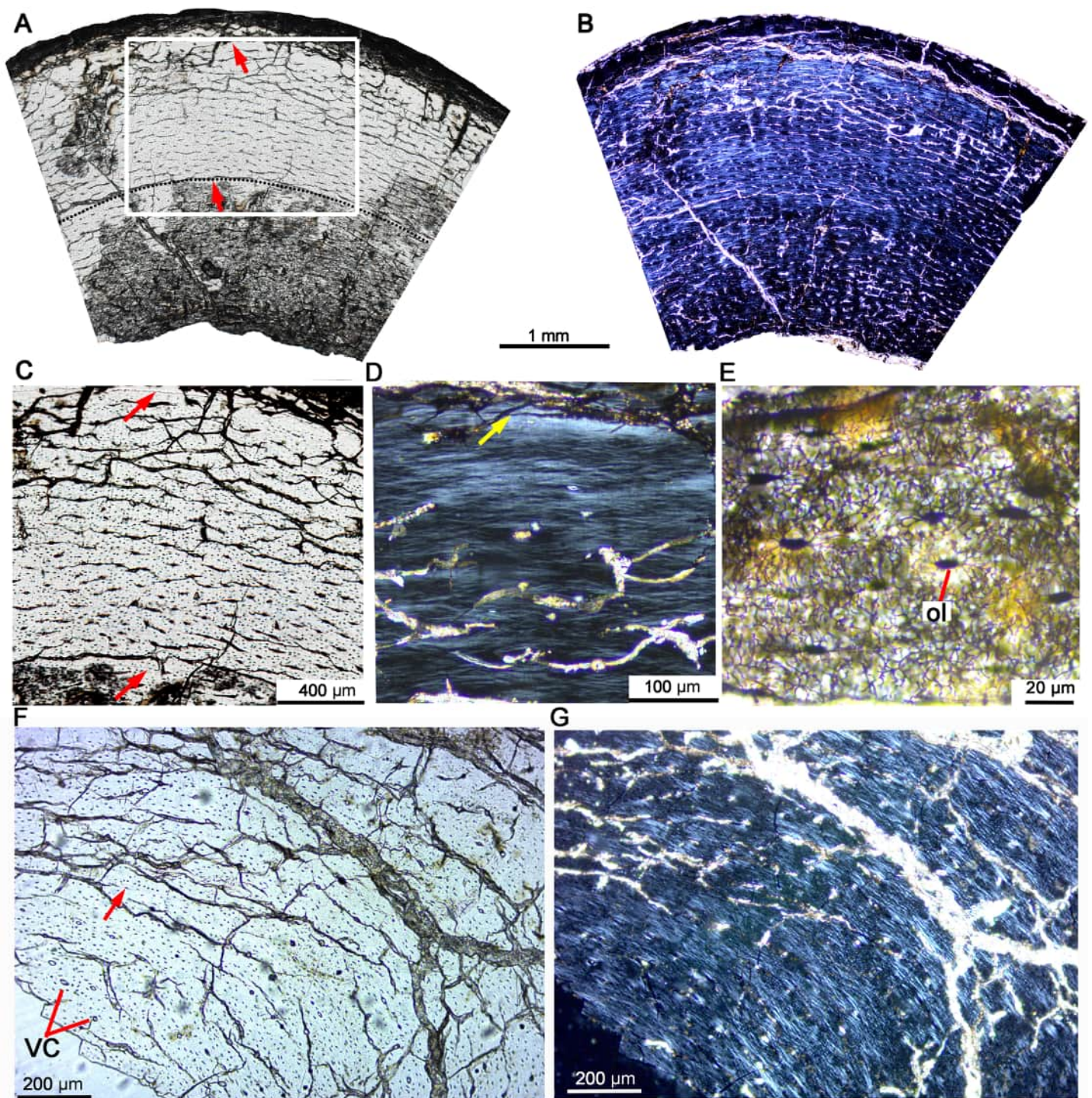


Figure 2 Bone microstructure of the tibia and fibula in early juvenile *Yinlong downsi* IVPP V18677. (A–E) Tibia. Bone microstructure of tibia under normal (A) and polarized (B) light. (C) Enlargement of the mid-cortex showing vascularization type and LAGs. (D) Enlargement of the outer cortex showing parallel-fibered bone tissue and the outer LAG. (E) Enlargement of the outer cortex showing osteocyte and dense canaliculi. (F, G) Fibula. Parallel-fibered bone tissue with longitudinal vascular canals under normal (F) and polarized (G) light. All arrows indicate LAGs. Abbreviations: vc, vascular canal; ol, osteocyte lacuna.

Full-size [DOI: 10.7717/peerj.18761/fig-2](https://doi.org/10.7717/peerj.18761/fig-2)

Table 2 Characteristic bone microstructure of the tibia in the three growth stages of *Yinlong downsii*.

| | Early juvenile | Late juvenile | Subadult | Adult |
|--|--------------------|-----------------------------|--|--|
| Specimen number | IVPP V18677 | IVPP V33266; IVPP V18678 | IVPP V18636; IVPP V33267; IVPP V18679; IVPP V18682 | IVPP V18683; IVPP V33268; IVPP V18637 |
| Primary osteons | Abundant | Abundant | Abundant | Abundant |
| Erosion cavity in the inner cortex | No | Yes | Yes | Yes |
| Secondary osteons | No | No | Few to abundant | Dense |
| Secondary remodeling | No | No | Yes | Yes |
| Endosteal bone | Absent | Absent or thin | Absent or thin | Absent or thin |
| Dominated bone tissue type | Fibrolamellar bone | Fibrolamellar bone | Fibrolamellar bone and Parallel-fibered bone | Fibrolamellar bone and parallel-fibered bone |
| Thickened and highly organized parallel-fibered bone in the outer cortex | No | No | Yes | Yes |
| Vascular canal shape | Longitudinal | Longitudinal and reticular | Longitudinal and reticular | Reticular |
| Preserved LAG number | 2 | 4–5 | 4–7 | 8–10 |
| Total LAGs | 1–3 | 4–5 | 6–10 | >11 |

Note:

Total LAGs denote the preserved LAG plus the estimated erosion LAGs.

and outer regions of the cortex exhibit dark colors under normal and polarized light. At higher magnification, dense oval-shaped osteocytes with complex canaliculi are clearly visible in the outer region of the tibial cortex (Fig. 2E). Osteocyte lacunae are abundant and randomly distributed throughout the cortex, yet they are organized in lines parallel to the LAGs. In the fibula, vascular density is relatively low compared to that of the tibia (Fig. 2F). The partial cortex consists of parallel-fibered bone tissue with longitudinal vascular canals (Fig. 2G). No bone remodeling is observed in the inner region. Three LAGs are present, indicating that the innermost LAG of the tibia may have been eroded due to the enlargement of the medullary cavity. The medullary cavity of the fibula is small.

Late juvenile stage

The late juvenile stage is represented by the tibia of IVPP V33266 (Table 2, Fig. 3), which has a femur length of approximately 155 mm. The vascular density throughout the cortex is notably high. The vascular organization is primarily characterized by reticular vascularization, although longitudinal vascularization is also abundant (Fig. 3A). Most vascular canals are encased in a thin layer of lamellar bone, forming primary osteons, while a few simple primary vascular canals and open vascular canals are observed near the periphery (Figs. 3B, 3C). No secondary osteons are present. Fibrolamellar bone tissue is predominant, but parallel-fibered bone is also common and highly organized near the LAGs (Figs. 3A, 3B). Four LAGs are visible circumferentially in the cortex, with the outermost LAG accompanied by a thin layer of highly organized parallel-fibered bones near the periphery (Figs. 3A, 3B). Osteocyte lacunae are oval or nearly round throughout most of the cortex, but they appear relatively flattened near the LAGs and in the outermost region. Sharpey's fibers are present in the outer cortex of the tibia (Fig. 3A). Bone tissue of the fibula consists of fibrolamellar bone with predominant longitudinal vascular canals, but

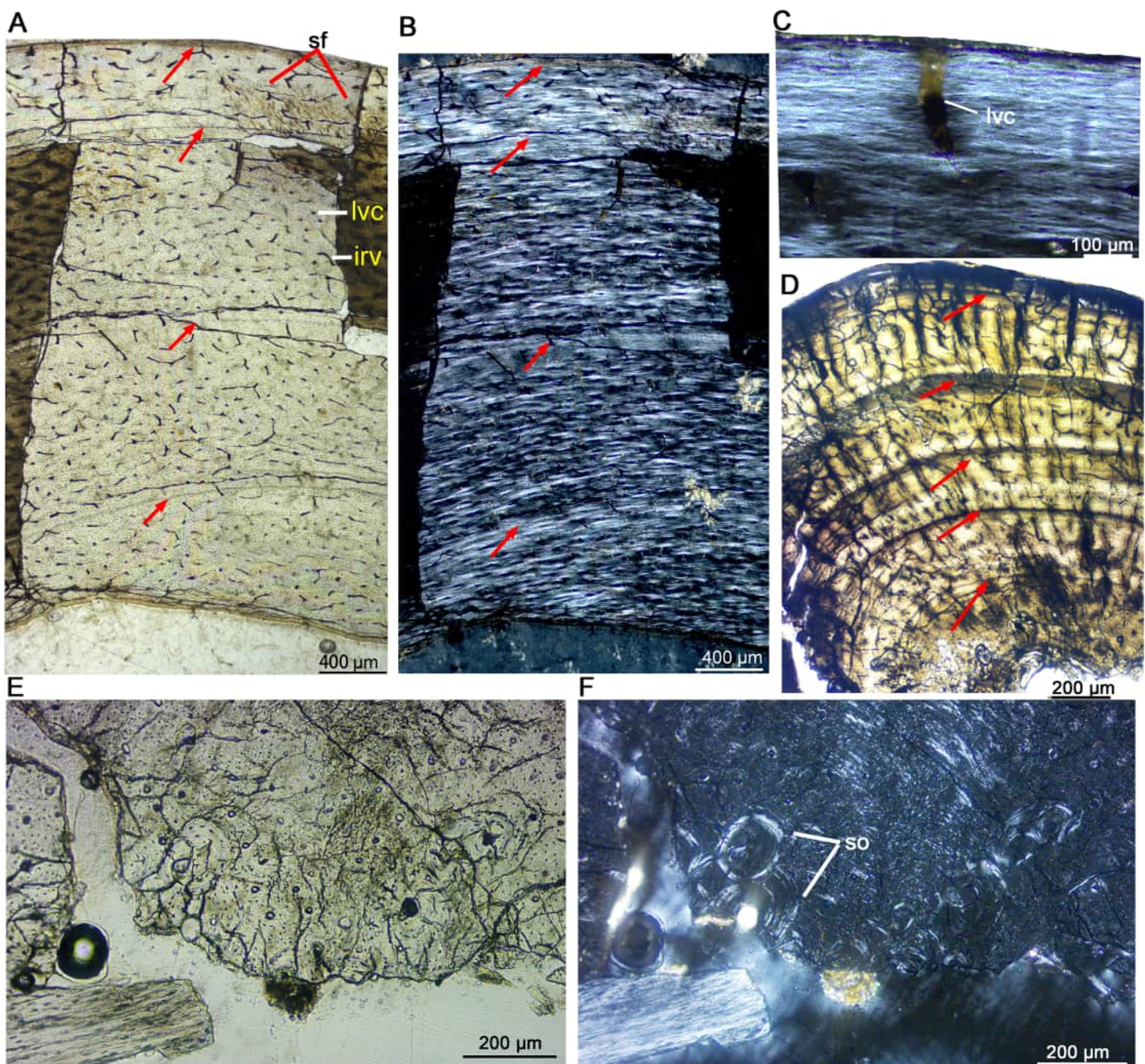


Figure 3 Bone microstructure of the limb bones in late Juvenile *Yinlong downsi* (IVPP V33266). (A–C) Tibia. Partial cortex under normal (A) and polarized (B) light; (C) Enlargement of the outermost cortex showing parallel-fibered bone and one vascular canal. (D) Partial cortex of one dorsal rib, showing LAGs. (E, F), Fibula. Bone microstructure in the innermost region under normal (E) and polarized (F) light, showing dense secondary osteons and partial endosteal bone tissue. All arrows indicate LAGs. Abbreviations: ira, irregular vascular canal; lvc, longitudinal vascular canal; sf, Sharpey's fibers; so, secondary osteons.

Full-size [DOI: 10.7717/peerj.18761/fig-3](https://doi.org/10.7717/peerj.18761/fig-3)

a few secondary osteons are observed in the innermost region (Figs. 3E, 3F). The sectional dorsal rib exhibits less bone remodeling compared to limb bones. It contains a small medullary cavity, a thin layer of endosteal bone, and five complete LAGs, indicating that the individual was at least 5 years old when it died (Fig. 3D).

IVPP V18678 is similar in size to IVPP V33266 (Table 1). The whole cross sections of the tibia and fibula were sampled. The cortex of the tibia is elliptical, with a maximum diameter of 16.5 mm and a minimum diameter of 13.5 mm (denoted as 16.5×13.5 mm). It consists of fibrolamellar bone with predominant longitudinal primary osteons (Figs. 4A, 4C). Four LAGs are visible in the cortex under normal light. Alternating woven bone (dark color) and parallel-fibered bone (bright color) are distinctly observable under polarized light (Fig. 4B). The distance between adjacent LAGs is relatively equal. Differing from IVPP V33266, the inner region of the tibial cortex forms many large resorption cavities and a thin layer of endosteal bone (Figs. 4C, 4D). In the fibula, dense secondary osteons are observed throughout the whole cortex (Figs. 4E–4G), and a thick layer of endosteal bone (about 100 μm) has formed in the innermost region (Figs. 4F, 4G).

Subadult stage

The subadult stage is represented by three specimens. IVPP V18636 has a femur length of about 178 mm (Table 1). The tibia, fibula, and rib were sectioned. The cortex of the tibia is elliptical, with a maximum diameter of 22.4 mm and a minimum diameter of 14.7 mm (Fig. 5). Most vascular canals are longitudinal, and there are also many irregular vascular canals (Figs. 5A–5D). The cortex consists of a large area of parallel-fibered bone tissue in its outer region (Fig. 5D). Four LAGs are distributed in the cortex, with the innermost two LAGs closely positioned, forming double LAGs (Fig. 5A). The distance between adjacent LAGs decreases towards the periphery. Remodeling of secondary osteons occurs in the innermost cortex (Figs. 5E, 5F).

The whole cross-section of the fibula is elliptical. Most of the vascular canals are longitudinal and irregular (Fig. 5G). The cortex consists of fibrolamellar bone tissue in the middle and lateral regions, but remodeling of dense secondary osteons is present in the inner region (Fig. 5G). The cortex of the rib mainly consists of a parallel fibered bone matrix. Seven LAGs are visible (Fig. 5H). Secondary osteons are distributed in the inner region, medial to the second LAG. The medullary cavity of the rib is very small and it seems that there is no erosion of LAG, suggesting that the individual was 7 years old when it died.

In IVPP V18679, the whole cross-section of the tibia is subtriangular (20.6×17.4 mm). The average thickness of the cortex is about 3.7 mm. The medullary cavity is very large. The vascular canals are abundant and irregular, forming reticular fibrolamellar bone tissue (Fig. 6A). Primary osteons are abundant, and dense secondary osteons concentrate at the corner of the cross section (Figs. 6C, 6D). Additionally, vascular canals near these secondary osteons are parallel and extend toward the corner (Fig. 6C). Five LAGs are distinctly visible, with their distances gradually decreasing toward the periphery (Figs. 6A, 6B). The outermost two LAGs are very close to each other. The cross section of a dorsal rib from IVPP V18679 is subcircular (6.7×4.3 mm). Vascular canals are abundant and longitudinal. The inner region contains several large erosion cavities (Fig. 6D), and a few secondary osteons are present. Four LAGs are clearly observable. A thin layer of endosteal bone is evident in the innermost region.

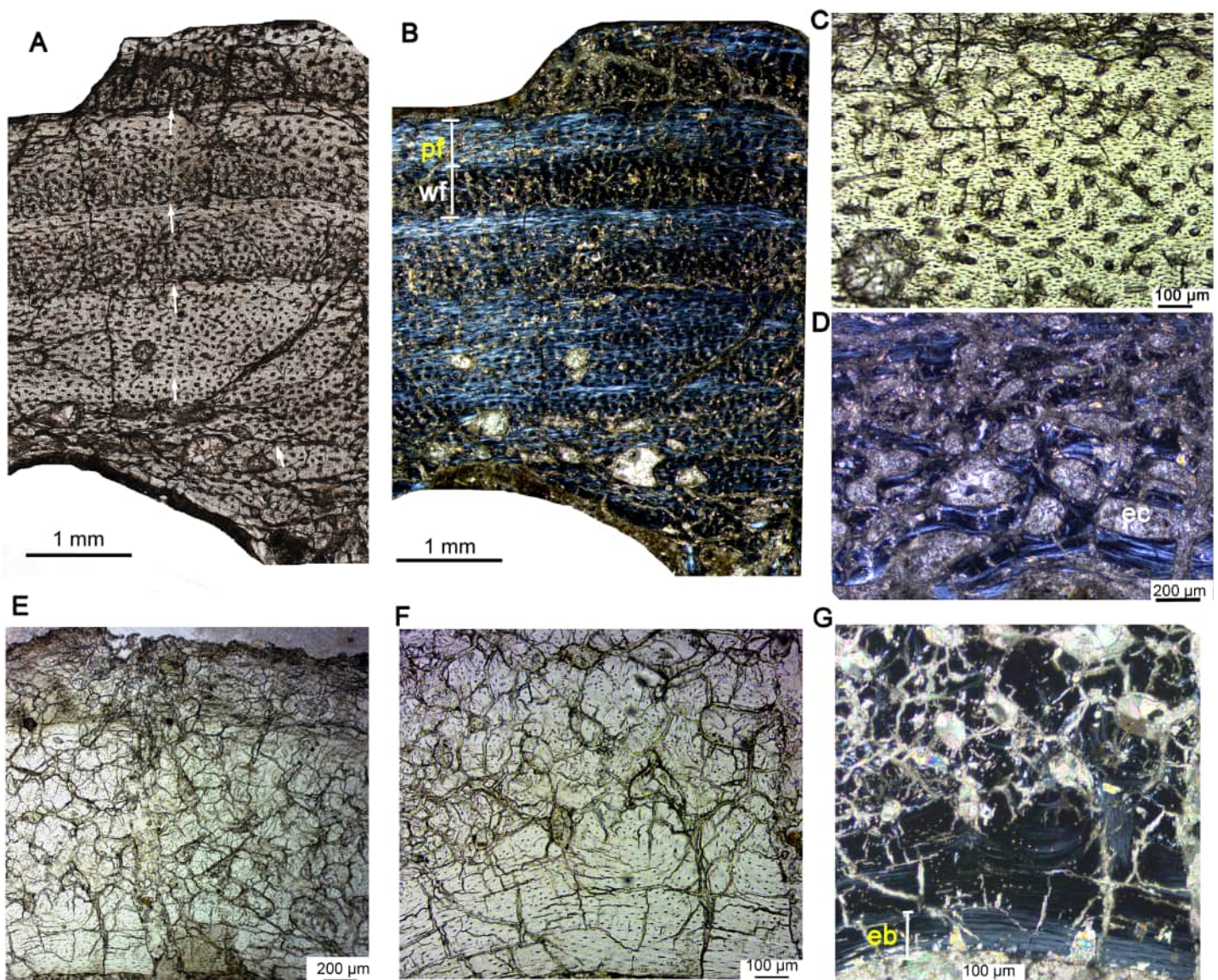


Figure 4 Bone microstructure of the limb bones in late Juvenile *Yinlong downsi* IVPP V18678. (A–D) Tibia. Partial cortex under normal (A) and polarized (B) light. (C) Enlargement of the mid cortex under normal light, showing longitudinal vascular canals. (D) Enlargement of the inner cortex under polarized light, showing erosion cavities. (E–G) Fibula. (E) Partial cortex under normal light. Enlargement of the inner cortex under normal (F) and polarized (G) light, showing dense secondary osteons and a wide endosteal layer. Abbreviations: eb, endosteal bone; ec, erosion cavity; pf, parallel fibered bone; wf, woven-fibered bone. All arrows indicate LAGs. [Full-size !\[\]\(e4c51d9db35ee9651ed60d72acdb782c_img.jpg\) DOI: 10.7717/peerj.18761/fig-4](https://doi.org/10.7717/peerj.18761/fig-4)

In IVPP V18682, the whole cross section of the fibula is elliptical (9.3×5.5 mm) (Fig. 7A). Vascular canals are mainly longitudinal. Primary osteons are distributed in the mid and outer regions. Dense radial canals are present in the outer cortex, surrounded by a thin layer of lamellar bone tissue (Fig. 7). The dense radial canals are similar to the pathological bone microstructure of an extant turkey vulture and non-avian dinosaur from Transylvania (Chinsamy & Tumarkin-Deratzian, 2009). A few secondary osteons and large erosion cavities are observed in the inner region (Figs. 7D, 7E). Seven LAGs are

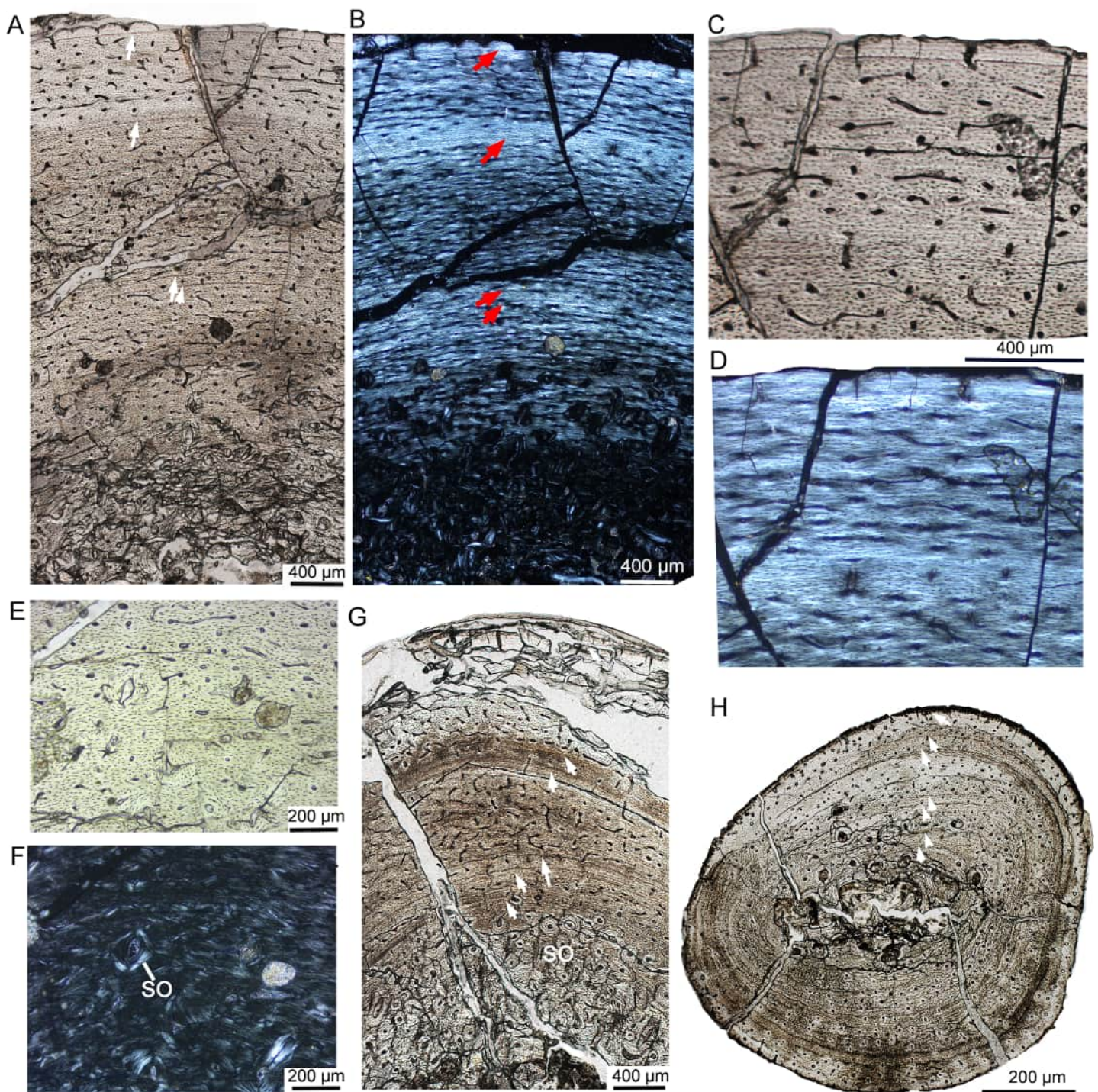


Figure 5 Bone microstructure of the limb bones in subadult *Yinlong downsi* IVPP V18636. (A–F) Tibia. Partial cortex under normal (A) and polarized (B) light. Enlargement of the outer cortex showing LAGs and parallel-fibered bone under normal (C) and polarized (D) light. Bone microstructure of the innermost region under normal (E) and polarized (F) light, showing dense secondary osteons. (G) Partial cortex of the fibula. (H) Whole cross-section of the dorsal rib. All arrows indicate LAGs. Abbreviation: so, secondary osteon.

Full-size  DOI: 10.7717/peerj.18761/fig-5

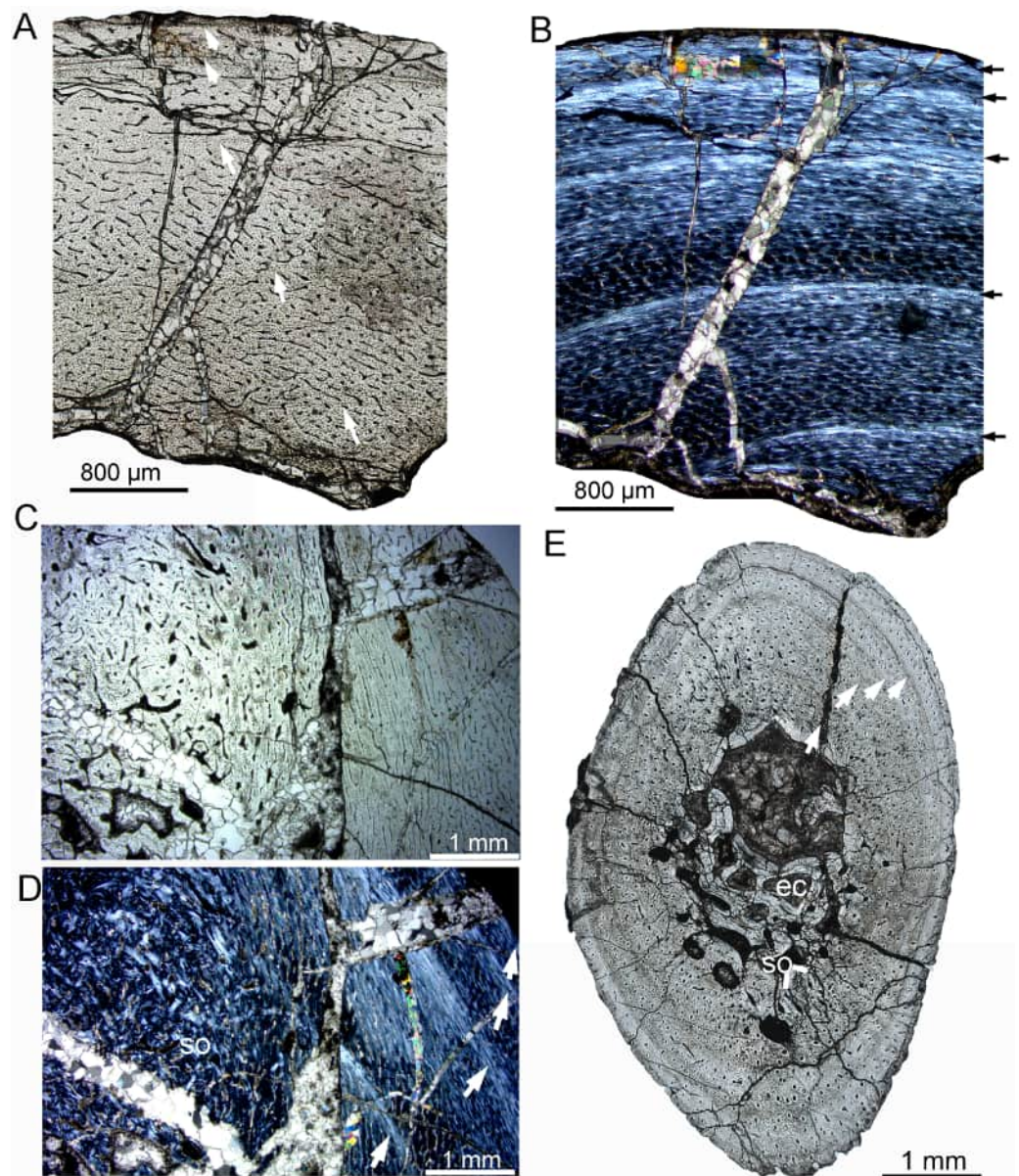


Figure 6 Bone microstructure of the tibia and rib in subadult *Yinlong downsi* IVPP V18679. (A–D) Tibia. Partial cortex under normal (A) and polarized (B) light. Bone remodeling in the inner cortex under normal (C) and polarized (D) light. (E) Whole cross-section of the dorsal rib. All arrows indicate LAGs. Abbreviations: ec, erosion cavity; so, secondary osteon. [Full-size](#) DOI: 10.7717/peerj.18761/fig-6

shown in the cortex. The inner six LAGs are evenly spaced and the seventh LAG is distributed near the periphery.

Adult

The adult stage was represented by two individuals, IVPP V18683 and IVPP V18637 (Table 2). Vascular canals are reticular at the middle region but predominantly longitudinal in the outer region (Fig. 8A). Vascular canals decrease in number towards the periphery, and scarce vascular canals are shown near the periphery, suggesting a very slow

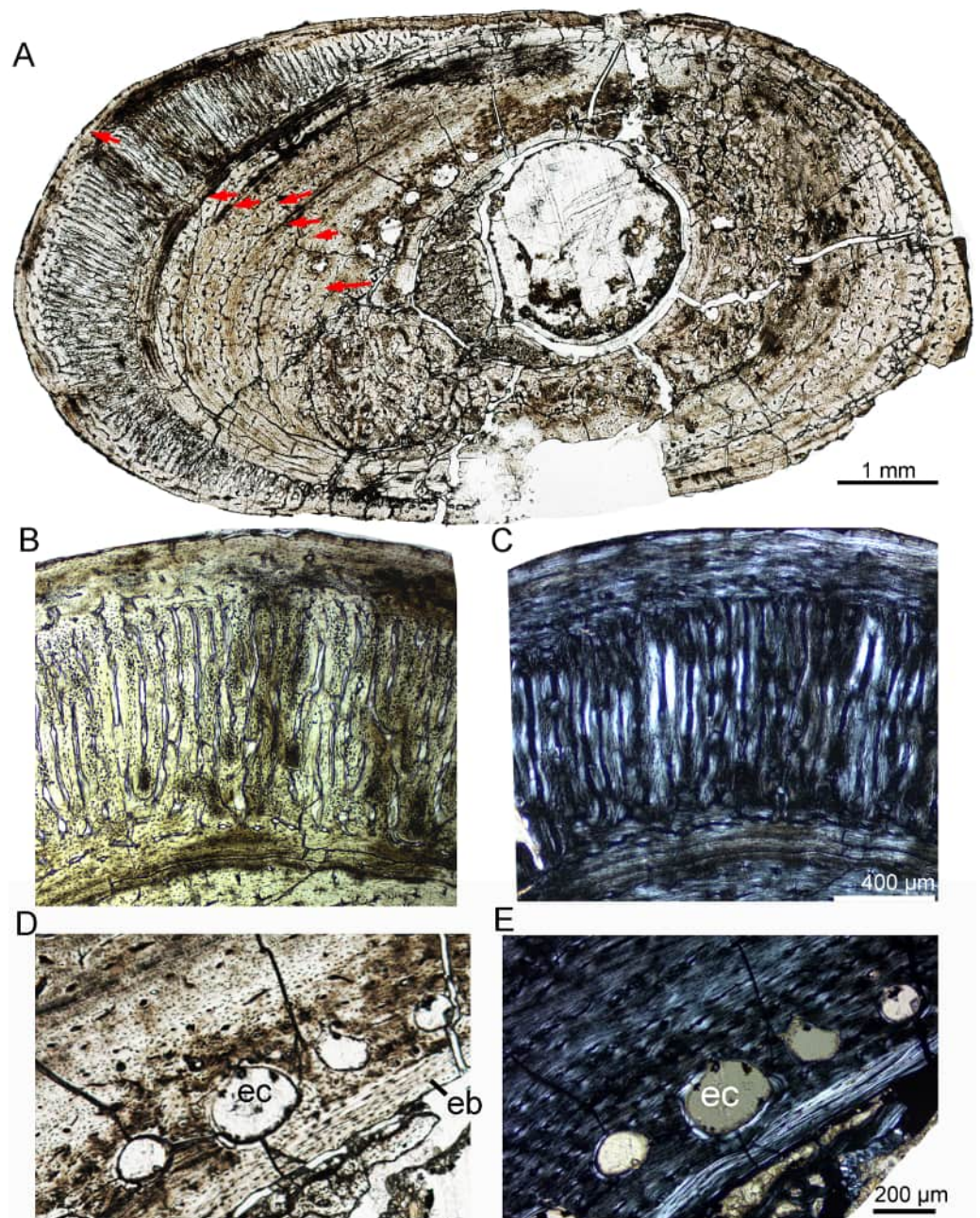


Figure 7 Bone microstructure of the fibula in subadult *Yinlong downsi* IVPP V18682. (A) Whole cross-section; Enlargement of the dense radial canals (likely pathological bone) under normal (B) and polarized (C) light. Enlargement of the innermost region under normal (D) and polarized (E) light. All arrows indicate LAGs. Abbreviations: eb, endosteal bone; ec, erosion cavity.

Full-size  DOI: [10.7717/peerj.18761/fig-7](https://doi.org/10.7717/peerj.18761/fig-7)

growth rate at the time of death (Figs. 8E, 8F). The cortex of the tibia mainly consists of fibrolamellar bone in the mid-region and a thick layer of parallel-fibered bone in the outer region (Figs. 8A, 8B). Eight and ten LAGs are visible in the cortex of IVPP V18683 and IVPP V18637, respectively. The distance between adjacent LAGs is very close near the periphery (Fig. 8A). Dense secondary osteons are observed in the inner cortex (Figs. 8C,

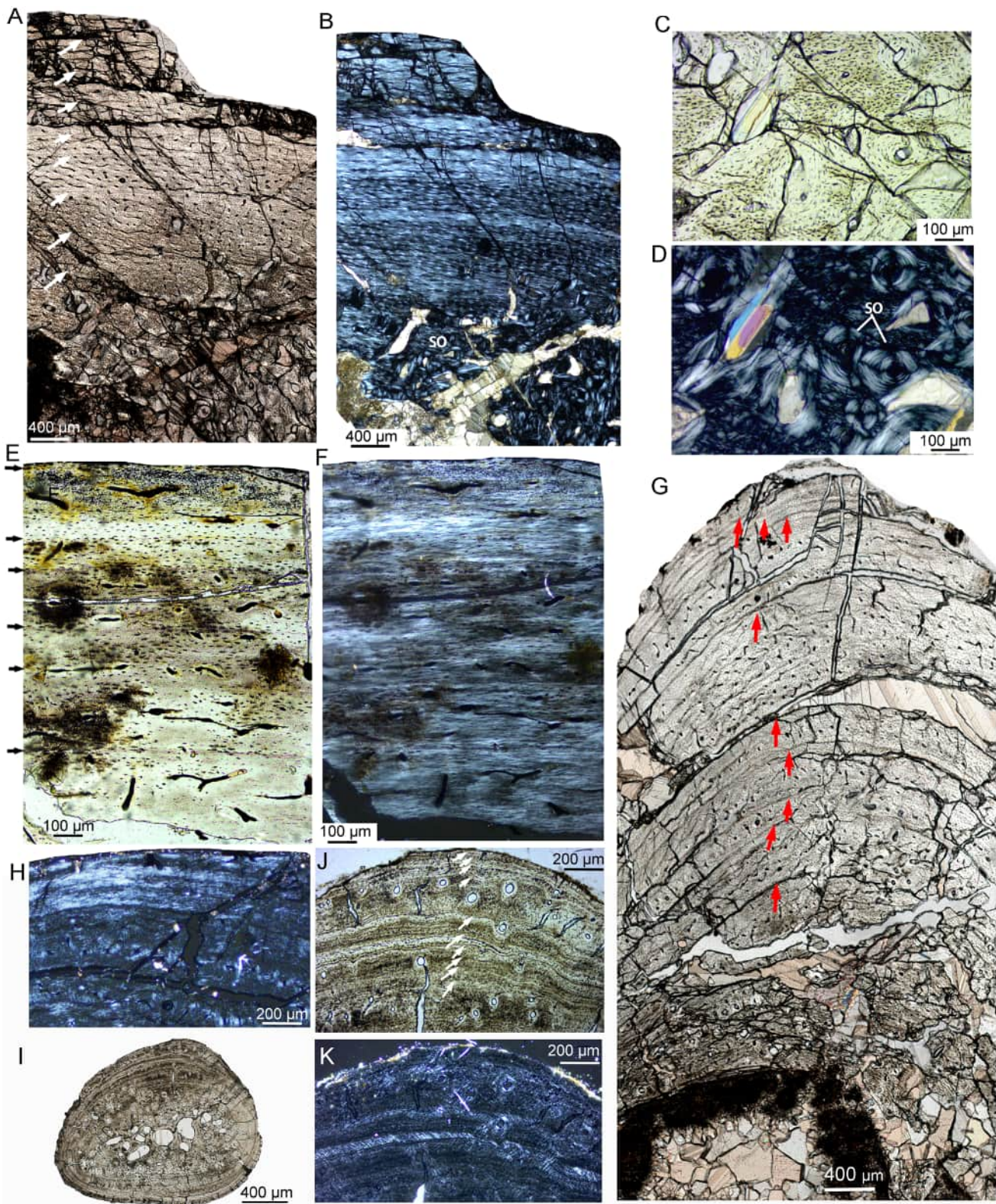


Figure 8 Bone microstructure of limb bones and rib in adult *Yinlong downsi*. (A–D) Tibia of IVPP V18683. Partial cortex under normal (A) and polarized light (B). Enlargement of the innermost region showing dense secondary osteons under normal (C) and polarized light (D). Tibia of IVPP V18637 under normal (E) and polarized (F) light. (G, H) Fibula of IVPP V18683. (G) Partial cross section under normal light, showing longitudinal

Figure 8 (continued)

vascular canals and LAGs. (H) Outermost region under polarized light showing lamellar bone tissue without vascular canal. (I–K) Rib of IVPPV18683. (I) Whole cross section of a dorsal rib. Partial bone section showing LAGs and secondary osteons in outer cortex under normal (J) and polarized (K) light. All arrows indicate LAGs. Abbreviation: so, secondary osteon.

Full-size  DOI: [10.7717/peerj.18761/fig-8](https://doi.org/10.7717/peerj.18761/fig-8)

8D). A thin layer of endosteal bone is observed in the innermost cortex of IVPP V18683 but is absent in that of IVPP V18637. The medullary cavity is relatively large.

The fibula of IVPP V18683 preserved nine LAGs (Fig. 8G). Vascular canals are predominantly longitudinal. The periphery consists of three closely packed LAGs, forming a wide lamellar bone devoid of vascular canals (Figs. 8G, 8H). The cortex of the rib mainly consists of parallel-fibered bone tissue (Figs. 8I–8K). The vascular canals are longitudinal and decrease in number towards the periphery. The inner region consists of dense secondary osteons, while only a few secondary osteons are observed in the outer cortex (Figs. 8J, 8K). Ten LAGs are visible in the cortex and are tightly articulated (Fig. 8J). The inner LAGs are partially erased by secondary osteons. The distance between adjacent LAGs decreases toward the periphery, with the outermost four LAGs being in very close proximity to each other.

DISCUSSION

Variation of bone tissue in *Yinlong downsii*

Generally, all of the sampled sections display parallel-fibered “fibrolamellar” bone that is interrupted by LAGs, as in many small dinosaurs, such as *Jeholosaurus*, *Lesothosaurus*, *Orodromeus*, and *Psittacosaurus* (Horner et al., 2009; Knoll, Padian & de Ricqlès, 2010; Zhao et al., 2019; Han et al., 2020). The parallel-fibered “fibrolamellar” bone is also reported in *Triceratops*, in which the bone matrix is not strictly woven but is often characterized by parallel-fibered bone (de Rooij et al., 2024). Similar bone tissue defined as “modified laminar bone” is observed in some sauropods, indicating relatively slower growth rates than that of typical fibrolamellar bone (Klein et al., 2012).

The variation of bone tissue is observed during ontogeny and different skeletal elements. For the tibia, the juvenile stage generally has a longitudinal vascular pattern, followed by the subadult stage with a reticular vascular pattern and dense secondary osteons in the inner part of the cortex. The adult is marked by thick parallel fibered bone with fewer vascular canals and closely compact LAGs but no EFS (external fundamental system). Similar ontogenetic variations are also observed in most small to medium-sized dinosaurs (e.g., *Jeholosaurus*, *Psittacosaurus*), but vary in different taxa. In *Psittacosaurus*, secondary remodeling happened in the relatively late growth stage, and endosteal bone is more complete in the adult (Zhao et al., 2019). Specifically, parallel-fibered bone tissue is prominent through ontogeny and an EFS is present in the small theropod dinosaur *Masiakasaurus* (Lee & O’Connor, 2013).

For the fibula and ribs, the vascular pattern is mainly longitudinal. Bone remodeling happens earlier in the fibula than in the tibia. This differs from the condition observed in *Jeholosaurus*, in which the fibula is less remodeled and preserves the complete endosteal bone and LAGs (Han et al., 2020).

Both the tibia and fibula of *Yinlong* have relatively larger medullary cavities than those of the ribs. The dorsal ribs are less remodeled and preserve the most complete number of LAGs compared to other elements, making them better for age estimation than other elements. This is also the case that was proved in many dinosaurs and crocodylomorphs, and the proximal end of the rib shaft is the best sample position and preserved the nearly complete growth record (Waskow & Sander, 2014; Waskow & Mateus, 2017). However, age estimation based on dorsal ribs may not be very accurate in adult individuals. For example, in the adult individual of *Yinlong*, the cortex of the dorsal rib is composed of lamellar bone, and many LAGs and other growth marks are concentrated near the periphery and sometimes they are not easy to discern (Fig. 8). In addition, strong bone remodeling obscuring LAGs was found in the largest rib of *Pachyrhinosaurus* (Hedrick et al., 2020). Therefore, it is not enough to estimate the longevity in the late ontogenetic stage only according to the bone microstructure of the dorsal rib. Cross sections of limb bones such as the femur, tibia, and fibula, are also necessary for accurate age estimation.

Endosteal bone is more common in the fibulae than other elements. In most elements, the distance of adjacent LAGs gradually decreases towards the periphery. However, double LAGs are present in the tibia of subadult IVPP V18636. Double or triple LAGs are commonly present in extant and extinct taxa, including amphibians, reptiles, birds, and mammals (Cullen et al., 2021; Han, Zhao & Liu, 2021). These growth marks are usually considered to be formed in 1 year. The occurrence of multiple LAGs was regarded as a harsh environmental condition or aestivation (Köhler & Moyà-Solà, 2009; Sanchez et al., 2010; Cullen et al., 2021). However, sometimes the double LAGs are not easy to identify, especially near the periphery. Cullen et al. (2021) suggested tracing the full circumference of a section to confirm if they were completely distinct, but a whole cross-section is difficult to make in large bones such as sauropods, hadrosaurs, and ceratopsids. The longevity of a taxon could be overestimated if the multiple LAGs are not recognized correctly. A thick layer of porous radial canals are seen in a fibula of *Yinlong* (Fig. 7), and they are also seen in the bone tissue of tibiae of *P. mongoliensis* at approximately 8 years of age (Erickson & Tumanova, 2000). However, dense radial canals are not seen in any normal bone tissue of *P. lujiatunensis* and *Koreaceratops* but are observed in the fractured bone of *Psittacosaurus*, and were regarded as a pathology (Chinsamy & Tumarkin-Deratzian, 2009; Hedrick et al., 2016; Zhao et al., 2019). Nevertheless, dense radial canals were also reported in the tibia of a late growth stage in *P. mongoliensis* and were supposed to reflect osseous drifting (Erickson & Tumanova, 2000).

The life history of *Yinlong*

The overall growth pattern of *Yinlong* is S-shaped as in most extant vertebrates and other dinosaurs (Fig. 9) (Zullinger et al., 1984; Erickson, Rogers & Yerby, 2001). The perinatal ontogenetic stage is not preserved in *Yinlong*. According to body mass estimation by Campione et al. (2014), the growth rates for *Yinlong* are up to 17.4 g/day at the age of three, increased up to 24.6 g/day at 5 years old, and gradually decreased to 1.6 g/d at the age of 12. The maximum growth rate is 14.6 g/day based on body mass estimation by the formula of

Anderson, Hall-Martin & Russell (1985). *Yinlong* reaches its maximum growth rates at the juvenile stage as in other dinosaurs. The maximum growth rate of *Yinlong* is similar to that of other small dinosaurs, such as *Psittacosaurus* (13.8 g/day) (Erickson & Tumanova, 2000), *Dysalotosaurus* (18.6 g/day), *Coelophysis* (11.2 g/day), *Saurornitholestes* (14.1 g/day), and *Troodon* (16.6 g/day) and is faster than most extant reptiles but slower than large-sized dinosaurs, extant mammals and avian taxa (Fig. 10) (Hübner, 2012; Grady et al., 2014). The body size of ceratopsians increased during their evolution but the number of LAGs did not increase correspondingly but decreased in late diverging ceratopsids, suggesting that the maximum growth rate was accelerating during the evolution of ceratopsians.

In *Yinlong*, sexual maturity occurs at approximately 6 years old based on a slowdown of growth rate (Fig. 9) and correlates with a transition of bone tissue from fibrolamellar bone to a parallel-fibered bone in the outer cortex seen in subadult and adult stages (Figs. 5–8). This is earlier than those of *Psittacosaurus* (Erickson et al., 2009) and some iguanodontians, such as *Dysalotosaurus* (Hübner, 2012) and *Tenontosaurus* (Lee & Werning, 2008), but older than the ceratopsid *Einosaurus* (3–5 years old) (Reizner, 2010), many small ornithopods such as *Jeholosaurus* (Han et al., 2020), *Orodromeus* (Horner & Goodwin, 2009) and hadrosaur *Maiasaura* (Woodward et al., 2015). It seems that the attainment of sexual maturity is earlier in ceratopsids than in early-diverging ceratopsians. However, in ornithopods, the attainment of sexual maturity is delayed from small ornithopods to iguanodontians but is earlier in hadrosaurs (Lee & Werning, 2008; Woodward et al., 2015; Han et al., 2020). In summary, both these clades have earlier sexual maturity in late-diverging taxa.

The presence of EFS usually indicates a fully grown stage in vertebrates and has been found in extant mammals, pterosaurs, birds, and all kinds of non-avian dinosaurs, such as *Troodon*, *Europasaurus*, *Apatosaurus*, *Maiasaura*, and *Stegosaurus* (Varricchio, 1993; Horner, De Ricqlès & Padian, 2000; Chinsamy-Turan, 2005; Sander et al., 2006; Klein & Sander, 2008; Hayashi, Carpenter & Suzuki, 2009; Bertozzo et al., 2021). EFS was also found in Pseudosuchia lineage, such as the American alligator and the aetosaur *Aetosauroides scagliai*, suggesting that determinate growth is shared by Archosauria (Woodward, Horner & Farlow, 2011; Rainwater et al., 2022; Ponce, Desojo & Cerda, 2023). The absence of EFS in our thin sections suggests that the largest sampled individual of *Yinlong* is still not fully grown. However, the closely-spaced LAGs and parallel-fibered bone all indicate nearly maximum body size.

Comparison of bone microstructure between *Yinlong* and other ceratopsians

Psittacosaurus is more derived than *Yinlong*, and the bone histology of three species of the former has been well studied, including *P. mongoliensis*, *P. lujiatunensis* and *P. sibiricus* (Erickson & Tumanova, 2000; Zhao et al., 2019; Skutschas et al., 2021). They all consist of fibrolamellar bone with predominant longitudinal and reticular vascular canals in tibiae and fibulae, as in *Yinlong* (File S2). Thick parallel fibered bone layers are shown in the outer cortex of the late ontogenetic stage (subadult) of *P. lujiatunensis* and *P. sibiricus*, but

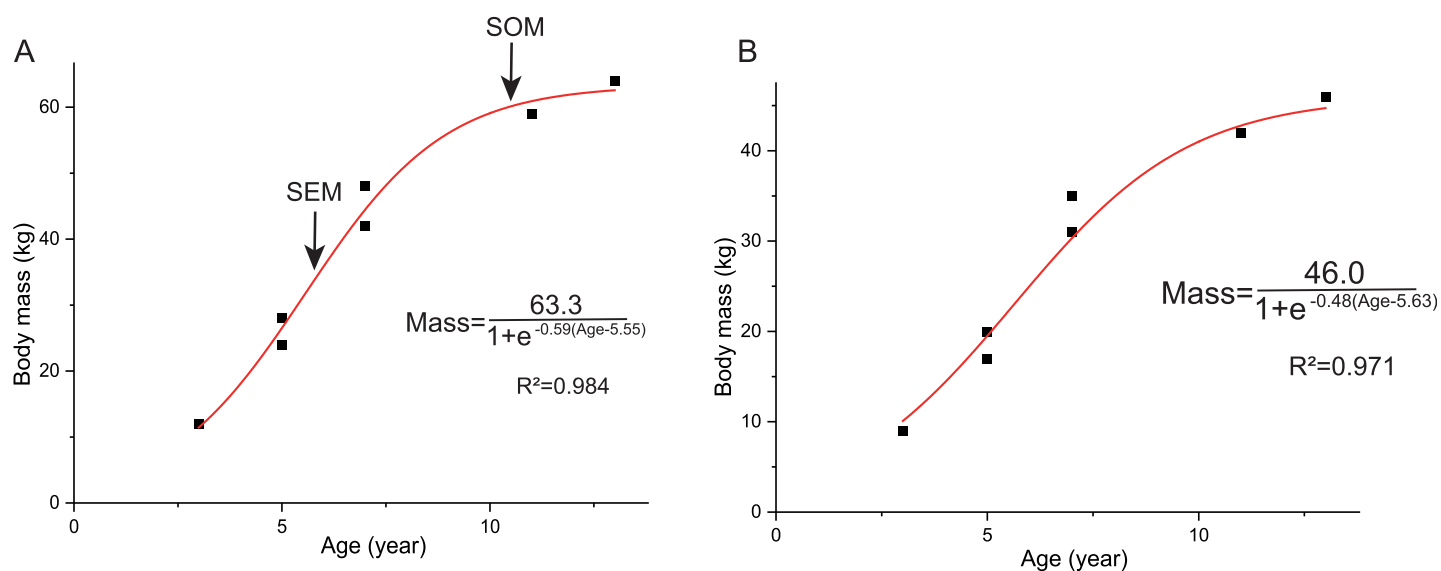


Figure 9 Growth curves (in red) of *Yinlong downsii*. The sigmoidal equation is used here to describe its growth pattern. (A) Body mass estimated by Campione et al. (2014); (B) Body mass estimated by Anderson, Hall-Martin & Russell (1985). Abbreviations: SEM, sexual maturity; SOM, somatic maturity. Full-size [DOI: 10.7717/peerj.18761/fig-9](https://doi.org/10.7717/peerj.18761/fig-9)

it is absent in the largest individual of *P. mongoliensis* (estimated to be about 9 years old) (Erickson & Tumanova, 2000). In addition, erosion bays are present in the early stage of the tibiae in *Yinlong*, *P. lujiatunensis* and *P. sibiricus*, but are only observed in the tibia of an eight-year-old specimen in *P. mongoliensis* (Erickson & Tumanova, 2000). Therefore, the bone microstructure of *Yinlong* is more similar to those of *P. lujiatunensis* and *P. sibiricus* than *P. mongoliensis*, and the largest known individual of *P. mongoliensis* is still histologically immature. However, secondary remodeling is shown in the subadult stage of *Yinlong*, as in *P. sibiricus*, but it only appeared in the largest individual of *P. lujiatunensis* (Zhao et al., 2013, 2019; Skutschas et al., 2021).

Radiating reticular vascularization, which is suggested to have rapid growth rates, was observed in the limb bones of *Psittacosaurus*, but is absent in tibial bone sections of *Yinlong*, suggesting the latter has a relatively lower growth rate. A thin layer of endosteal bone is present in the tibia of *Yinlong*, and it is thicker in the fibula, as in the condition of *P. lujiatunensis* (Zhao et al., 2019). However, no endosteal bone is found in the largest specimen of *Yinlong*, unlike that of *P. lujiatunensis*, which preserved a complete endosteal bone in adult individuals (Zhao et al., 2019). It seems that the endosteal bone may be eroded by the expansion of the medullary cavity in the tibia of adult individuals of *Yinlong*. LAGs are clearly observed in the early stage of *Yinlong*, as in *Psittacosaurus* (Erickson & Tumanova, 2000; Zhao et al., 2013, 2019) and many other small dinosaur bones (Chinsamy-Turan, 2005; Han et al., 2020).

Likewise, *Koreaceratops* is a small non-coronosaur neoceratopsian and more derived than *Yinlong* and *Psittacosaurus* (Lee, Ryan & Kobayashi, 2011; Morschhauser et al., 2018b). The length of preserved caudal vertebrae and partial pelvic girdle is less than 1 m, suggesting a small body size, but it may reach the subadult stage according to bone

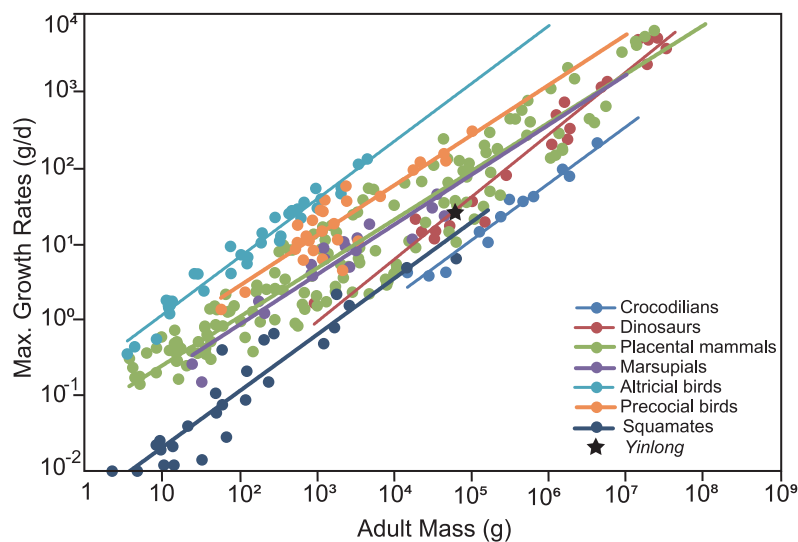


Figure 10 Comparison of the maximum growth rate of *Yinlong* with other dinosaurs and extant animals. *Yinlong* is located at the regression line of dinosaurs.

Full-size  DOI: 10.7717/peerj.18761/fig-10

microstructure (Lee, Ryan & Kobayashi, 2011; Baag & Lee, 2022). The fibula shows similar longitudinal and reticular vascular canals as those of *Yinlong* and *Psittacosaurus*. However, the tibia of *Koreaceratops* consists of longitudinal vasculature with circumferentially elongated osteon canals, and no LAG is observed. Instead, alternative zones and annuli is detected in the tibia. LAGs are present in the outermost part of the *Koreaceratops* right fibula. The degree of bone remodeling in the *Yinlong* tibia is lower than in the fibulae, as in the condition of *Koreaceratops* (Baag & Lee, 2022). Massive remodeling is reported in the *Koreaceratops* fibula which may be a result of a thin section near the proximal end. Osseous drift happens in the fibula of *Yinlong*, and it is also present in *Psittacosaurus* (Erickson & Tumanova, 2000; Zhao et al., 2019) and *Koreaceratops* (Baag & Lee, 2022), but the latter have heavier bone drift by the presence of anteromedial erosion rooms deep into the mid-cortex.

Cerasinops is a small non-coronosaur neoceratopsian that is closely related to *Koreaceratops*. It is possibly bipedal as in other early diverging ceratopsians (Chinnery & Horner, 2007). Both the hindlimb and forelimb of *Cerasinops* were sampled to study bone microstructure, and they display different bone tissue types (Chinnery & Horner, 2007). The humerus mainly contains longitudinal vascular canals, whereas they are more circumferential in the tibia. The latter differs from the vascular pattern of *Yinlong* and *Psittacosaurus* in which longitudinal and reticular canals are dominated. Seven LAGs are observed in the tibia, femur, and humerus but no evidence of an avascular external fundamental system, suggesting the sampled individual of *Cerasinops* is not fully grown.

On the other hand, *Protoceratops* is a small quadrupedal coronosaur neoceratopsian from the Upper Cretaceous of East Asia, falling outside ceratopsoids (Morschhauser et al., 2018b). Unlike the bone microstructure of *Yinlong*, *Protoceratops* displays a prevailing longitudinal vascularization pattern and is mainly comprised of alternating zones of

parallel-fibered and woven bone in their humeri, femora, and tibiae (Fostowicz-Frelik & Słowiak, 2018). Bone tissue of *Protoceratops* fibula is more similar to those of *Yinlong*. LAGs and annuli were only observed in the fibula of *Protoceratops*. The level of bone remodeling in the fibula is higher than in the tibia, contrasting to those of basal ornithomimid dinosaurs such as *Jeholosaurus* (Han et al., 2020). A large density of Sharpey's fibers was observed in the frill and limb bones of *Protoceratops* (Fostowicz-Frelik & Słowiak, 2018), but they are rare in the bone tissue of *Yinlong*.

Bone histology of ceratopsids is best known in the chasmosaurine *Triceratops*, which differs from basal ceratopsians in many aspects (Baag & Lee, 2022; de Rooij et al., 2024). Limb bones consist of a mix of longitudinal and circumferential vascular canals. Alternating zones of parallel-fibered and woven bone are clearly seen in limb elements of *Triceratops*. Parallel-fibered bone appeared in the juvenile stage of *Triceratops*. Bone remodeling in *Triceratops* happened in a much earlier stage than early ceratopsians, whereas LAGs are observed only in a very late stage (de Rooij et al., 2024). In chasmosaurines *Utahceratops* and *Kosmoceratops*, vascular canals are longitudinal and reticular, and no LAGs are found in sampled juvenile and subadult individuals (Levitt, 2013). However, LAGs seem to be commonly preserved in centrosaurines (Reizner, 2010; Hedrick et al., 2020). More than five LAGs are present in the tibia of *Centrosaurus* which is similar in size to the samples of *Utahceratops* and *Kosmoceratops* (Levitt, 2013). A maximum of six LAGs are preserved in a rib of *Avaceratops* and five LAGs are observed near the periphery of the femur in *Yehuecauhceratops* (Hedrick et al., 2020). As many as 18 LAGs are preserved in the femur of *Pachyrhinosaurus* (Erickson & Druckenmiller, 2011). The vascular canal pattern of *Centrosaurus* is different from that of other ceratopsians by the cycled longitudinal and radial orientation in the tibia of *Centrosaurus*. Histological ontogenetic variation of the centrosaurine ceratopid *Einiosaurus* has been well studied based on 16 individuals. The tibiae consist of fibrolamellar bone made up of reticular and longitudinal osteons as in basal ceratopsians *Yinlong*. Radial vascular canals are observed in the early stage (>1 year old). Bone remodeling began after 1 year old, which is earlier than that of *Yinlong*. In addition, the growth rate of *Einiosaurus* is highest at 3 years old, which is earlier than those of *Yinlong* and *Psittacosaurus* (Erickson et al., 2009). However, the largest size of *Einiosaurus* is still unknown because the sample individuals were suggested to be less than 6 years old according to the number of LAGs.

LAGs are clear and common in all bone elements of *Yinlong*, as in *Psittacosaurus* (Erickson & Tumanova, 2000; Zhao et al., 2013, 2019) and many other dinosaur bones (Chinsamy-Turan, 2005; Han et al., 2020), whereas they are not obvious in more derived ceratopsian *Koreaceratops* (Baag & Lee, 2022) and *Protoceratops* and also some ornithomimids (e.g., *Dysalotosaurus*) and many sauropods (Sander et al., 2004; Hübner, 2012). In ceratopsids and sauropods, LAGs only appear in the very late ontogenetic stage (Sander et al., 2011; de Rooij et al., 2024). The regular development of LAGs in large body size of dinosaurs was interpreted as high seasonal stress due to higher food demands, migration, and altricial breeding behavior (Hübner, 2012).

In summary, during the evolution of ceratopsians, there is a discernible augmentation in growth rate, accompanied by an earlier attainment of sexual maturity. Additionally, both

bone remodeling and secondary remodeling were accelerated and intensified. There was a decrease in LAG deposition, whereas bone zonation became more pronounced and extensive. Although the body size of ceratopsians continued to increase throughout their evolution, their lifespan did not correspondingly extend, as indicated by the number of preserved LAGs. Therefore, the increase in growth rate likely plays a significant role in the evolution of the substantial body size observed in ceratopsians. The absence of LAGs during the early ontogenetic stages of large-sized ceratopsid dinosaurs suggests rapid and uninterrupted growth. The evolution of bone microstructure in ceratopsians parallels that of sauropods and ornithopods, where LAGs are typically preserved across all growth stages in early-diverging sauropodomorphs and ornithopods, but appear later (in subadult or adult stages) in late-diverging sauropods and hadrosaurs (Klein & Sander, 2008; Cerda et al., 2017; Han et al., 2020; Wosik & Evans, 2022). In contrast, non-avian theropod dinosaurs exhibit LAGs in the early stages of both small and large species, such as *Tyrannosaurus*, indicating an interrupted growth rate even during juvenile stages (Horner & Padian, 2004; Carr, 2020). D'Emic et al. (2023) argued that the large size of non-avian theropods was the result of both increasing growth rate and duration. These findings provide new information on the growth strategy underlying the evolution of ceratopsians.

CONCLUSIONS

This study investigates the bone histology of the earliest ceratopsian *Yinlong downsi* for the first time, and the results show that the cortex of limb bone mainly consists of fibrolamellar bone that is interrupted by LAGs and parallel-fibered bone. This is similar to *Psittacosaurus*, whereas in derived ceratopsians, there is usually no clear LAGs and bone remodeling happens earlier. The maximum growth rate of *Yinlong* is faster than extant reptiles but slower than extant mammals and avians. The growth curve of *Yinlong* suggests that it reached sexual maturity at about 6 years old, which is earlier than *Psittacosaurus*, but later than that of late-diverging ceratopsians. It seems that the large size of ceratopsids was a result of fast growth rates and they reached sexual maturity earlier than their ancestors.

ACKNOWLEDGEMENTS

We thank the members of the Sino-American expedition team for collecting the fossils studied herein, and Yuzheng Ke and Rui Wu for making thin sections. We thank the editor Blanca Moncunill-Solé and the two anonymous reviewers for their careful review and very useful comments on this manuscript.

ADDITIONAL INFORMATION AND DECLARATIONS

Funding

This study was supported by the National Natural Science Foundation of China (41972021, 42288201, 42372046, 42072008, 42272020). The funders had no role in

study design, data collection and analysis, decision to publish, or preparation of the manuscript.

Grant Disclosures

The following grant information was disclosed by the authors:

National Natural Science Foundation of China: 41972021, 42288201, 42372046, 42072008, 42272020.

Competing Interests

The authors declare that they have no competing interests.

Author Contributions

- Fenglu Han conceived and designed the experiments, performed the experiments, analyzed the data, prepared figures and/or tables, authored or reviewed drafts of the article, and approved the final draft.
- Qi Zhao conceived and designed the experiments, performed the experiments, authored or reviewed drafts of the article, and approved the final draft.
- Jinfeng Hu performed the experiments, analyzed the data, prepared figures and/or tables, and approved the final draft.
- Xing Xu conceived and designed the experiments, performed the experiments, authored or reviewed drafts of the article, and approved the final draft.

Data Availability

The following information was supplied regarding data availability:

The raw data is available in the [Supplemental Files](#).

Supplemental Information

Supplemental information for this article can be found online at <http://dx.doi.org/10.7717/peerj.18761#supplemental-information>.

REFERENCES

- Anderson JF, Hall-Martin A, Russell DA. 1985.** Long-bone circumference and weight in mammals, birds and dinosaurs. *Journal of Zoology* **207**(1):53–61
DOI [10.1111/j.1469-7998.1985.tb04915.x](https://doi.org/10.1111/j.1469-7998.1985.tb04915.x).
- Baag SJ, Lee Y-N. 2022.** Bone histology on *Koreaceratops hwaseongensis* (Dinosauria: Ceratopsia) from the Lower Cretaceous of South Korea. *Cretaceous Research* **134**:105150
DOI [10.1016/j.cretres.2022.105150](https://doi.org/10.1016/j.cretres.2022.105150).
- Becerra MG, Pol D, Rauhut OWM, Cerda IA. 2016.** New heterodontosaurid remains from the Cañadón Asfalto Formation: cursoriality and the functional importance of the pes in small heterodontosaurids. *Journal of Paleontology* **90**(3):555–577 DOI [10.1017/jpa.2016.24](https://doi.org/10.1017/jpa.2016.24).
- Benson RBJ, Hunt G, Carrano MT, Campione N. 2018.** Cope's rule and the adaptive landscape of dinosaur body size evolution. *Palaeontology* **61**(1):13–48 DOI [10.1111/pala.12329](https://doi.org/10.1111/pala.12329).
- Bertozzo F, Da Silva BC, Martill D, Marlene E, Vorderwuelbecke TA, Schouten R, Aquino P. 2021.** A large pterosaur femur from the Kimmeridgian, Upper Jurassic of Lusitanian Basin. *Portugal Acta Palaeontologica Polonica* **66**:815–825 DOI [10.4202/app.00858.2020](https://doi.org/10.4202/app.00858.2020).

- Butler RJ, Upchurch P, Norman DB. 2008.** The phylogeny of the ornithischian dinosaurs. *Journal of Systematic Palaeontology* **6**(1):1–40 DOI [10.1017/S1477201907002271](https://doi.org/10.1017/S1477201907002271).
- Campione NE, Evans DC, Brown CM, Carrano MT. 2014.** Body mass estimation in non-avian bipeds using a theoretical conversion to quadruped stylopodial proportions. *Methods in Ecology and Evolution* **5**(9):913–923 DOI [10.1111/2041-210X.12226](https://doi.org/10.1111/2041-210X.12226).
- Carr TD. 2020.** A high-resolution growth series of *Tyrannosaurus rex* obtained from multiple lines of evidence. *PeerJ* **8**(12):e9192 DOI [10.7717/peerj.9192](https://doi.org/10.7717/peerj.9192).
- Cerda IA, Chinsamy A, Pol D, Apaldetti C, Otero A, Powell JE, Martínez RN. 2017.** Novel insight into the origin of the growth dynamics of sauropod dinosaurs. *PLOS ONE* **12**(6):e0179707 DOI [10.1371/journal.pone.0179707](https://doi.org/10.1371/journal.pone.0179707).
- Chinnery BJ, Horner JR. 2007.** A new neoceratopsian dinosaur linking North American and Asian taxa. *Journal of Vertebrate Paleontology* **27**:625–641 DOI [10.1671/0272-4634\(2007\)27](https://doi.org/10.1671/0272-4634(2007)27).
- Chinsamy A, Tumarkin-Deratzian A. 2009.** Pathologic bone tissues in a turkey vulture and a nonavian dinosaur: Implications for interpreting endosteal bone and radial fibrolamellar bone in fossil dinosaurs. *The Anatomical Record* **292**(9):1478–1484 DOI [10.1002/ar.20991](https://doi.org/10.1002/ar.20991).
- Chinsamy-Turan A. 2005.** *The microstructure of dinosaur bone*. Baltimore: Johns Hopkins University Press.
- Cullen TM, Brown CM, Chiba K, Brink KS, Makovicky PJ, Evans DC. 2021.** Growth variability, dimensional scaling, and the interpretation of osteohistological growth data. *Biology Letters* **17**(11):20210383 DOI [10.1098/rsbl.2021.0383](https://doi.org/10.1098/rsbl.2021.0383).
- D’Emic MD, O’Connor PM, Sombathy RS, Cerda I, Pascucci TR, Varricchio D, Pol D, Dave A, Coria RA, Curry Rogers KA. 2023.** Developmental strategies underlying gigantism and miniaturization in non-avian theropod dinosaurs. *Science* **379**(6634):811–814 DOI [10.1126/science.adc8714](https://doi.org/10.1126/science.adc8714).
- de Rooij J, Lucassen SAN, Furer C, Schulp AS, Sander PM. 2024.** Exploring the ceratopsid growth record: a comprehensive osteohistological analysis of *Triceratops* (Ornithischia: Ceratopsidae) and its implications for growth and ontogeny. *Cretaceous Research* **154**(3):105738 DOI [10.1016/j.cretres.2023.105738](https://doi.org/10.1016/j.cretres.2023.105738).
- Donath K, Rohrer M. 2003.** Bone sectioning using the exakt system. In: *Handbook of Histology Methods for Bone and Cartilage*. Berlin, Germany: Springer, 243–252.
- Dong Z-M. 1989.** On a small ornithopod (*Gongbusaurus wucaiwansensis* sp.nov.) from Kelamaili, Juggar Basin, Xinjiang, China. *Vertebrata Palasiatica* **27**:140–146 DOI [10.19615/j.cnki.1000-3118.1989.02.010](https://doi.org/10.19615/j.cnki.1000-3118.1989.02.010).
- Dong Z-M, Azuma Y. 1997.** On a primitive neoceratopsian from the Early Cretaceous of China. In: Dong Z-M, ed. *Sino-Japanese Silk Road Dinosaur Expedition*. Beijing: China Ocean Press, 68–89.
- Erickson GM, Druckenmiller PS. 2011.** Longevity and growth rate estimates for a polar dinosaur: a *Pachyrhinosaurus* (Dinosauria: Neoceratopsia) specimen from the North Slope of Alaska showing a complete developmental record. *Historical Biology* **23**(4):327–334 DOI [10.1080/08912963.2010.546856](https://doi.org/10.1080/08912963.2010.546856).
- Erickson GM, Makovicky PJ, Inouye BD, Zhou C-F, Gao K-Q. 2009.** A life table for *Psittacosaurus lujiatunensis*: initial insights into ornithischian dinosaur population biology. *The Anatomical Record* **292**(9):1514–1521 DOI [10.1002/ar.20992](https://doi.org/10.1002/ar.20992).
- Erickson GM, Rogers KC, Yerby SA. 2001.** Dinosaurian growth patterns and rapid avian growth rates. *Nature* **412**(6845):429–433 DOI [10.1038/35086558](https://doi.org/10.1038/35086558).

- Erickson GM, Tumanova TA. 2000.** Growth curve of *Psittacosaurus mongoliensis* Osborn (Ceratopsia: Psittacosauridae) inferred from long bone histology. *Zoological Journal of the Linnean Society* **130**(4):551–566 DOI [10.1111/j.1096-3642.2000.tb02201.x](https://doi.org/10.1111/j.1096-3642.2000.tb02201.x).
- Fastovsky DE, Weishampel DB, Watabe M, Barsbold R, Tsogtbaatar K, Narmandakh P. 2011.** A nest of *Protoceratops andrewsi* (Dinosauria, Ornithischia). *Journal of Paleontology* **85**(6):1035–1041 DOI [10.1666/11-008.1](https://doi.org/10.1666/11-008.1).
- Fonseca AO, Reid IJ, Venner A, Duncan RJ, Garcia MS, Müller RT. 2024.** A comprehensive phylogenetic analysis on early ornithischian evolution. *Journal of Systematic Palaeontology* **22**(1):2346577 DOI [10.1080/14772019.2024.2346577](https://doi.org/10.1080/14772019.2024.2346577).
- Fostowicz-Frelik Ł, Słowiak J. 2018.** Bone histology of *Protoceratops andrewsi* from the Late Cretaceous of Mongolia and its biological implications. *Acta Palaeontologica Polonica* **63**:503–517 DOI [10.4202/app.00463.2018](https://doi.org/10.4202/app.00463.2018).
- Francillon-Viellet H, de Buffrénil V, Castanet J, Géraudie J, Meunier FJ, Dire JY, Zylberberg L, de Ricqlès A. 1990.** Microstructure and mineralization of vertebrate skeletal tissues. In: Carter JG, ed. *Skeletal Biomineralization: Patterns, Processes and Evolutionary Trends*. New York: Van Nostrand Reinhold, 471–530.
- Grady JM, Enquist BJ, Dettweiler-Robinson E, Wright NA, Smith FA. 2014.** Evidence for mesothermy in dinosaurs. *Science* **344**(6189):1268–1272 DOI [10.1126/science.1253143](https://doi.org/10.1126/science.1253143).
- Han F-L, Forster C, Clark J, Xu X. 2015.** A new taxon of basal ceratopsian from China and the early evolution of Ceratopsia. *PLOS ONE* **10**(2):e0143369 DOI [10.1371/journal.pone.0148689](https://doi.org/10.1371/journal.pone.0148689).
- Han F-L, Forster CA, Clark JM, Xu X. 2016.** Cranial anatomy of *Yinlong downsi* (Ornithischia: Ceratopsia) from the Upper Jurassic Shishugou Formation of Xinjiang, China. *Journal of Vertebrate Paleontology* **36**(1):e1029579 DOI [10.1080/02724634.2015.1029579](https://doi.org/10.1080/02724634.2015.1029579).
- Han F-L, Forster CA, Xu X, Clark JM. 2018.** Postcranial anatomy of *Yinlong downsi* (Dinosauria: Ceratopsia) from the Upper Jurassic Shishugou Formation of China and the phylogeny of basal ornithischians. *Journal of Systematic Palaeontology* **16**(14):1159–1187 DOI [10.1080/14772019.2017.1369185](https://doi.org/10.1080/14772019.2017.1369185).
- Han F-L, Zhao Q, Liu J. 2021.** Preliminary bone histological analysis of *Lystrosaurus* (Therapsida: Dicynodontia) from the Lower Triassic of North China, and its implication for lifestyle and environments after the end-Permian extinction. *PLOS ONE* **16**(3):e0248681 DOI [10.1371/journal.pone.0248681](https://doi.org/10.1371/journal.pone.0248681).
- Han F-L, Zhao Q, Stiegler J, Xu X. 2020.** Bone histology of the non-iguanodontian ornithomimid *Jeholosaurus shangyuanensis* and its implications for dinosaur skeletochronology and development. *Journal of Vertebrate Paleontology* **40**(2):e1768538 DOI [10.1080/02724634.2020.1768538](https://doi.org/10.1080/02724634.2020.1768538).
- Hayashi S, Carpenter K, Suzuki D. 2009.** Different growth patterns between the skeleton and osteoderms of *Stegosaurus* (Ornithischia: Thyreophora). *Journal of Vertebrate Paleontology* **29**:123–131 DOI [10.1671/039.029.0109](https://doi.org/10.1671/039.029.0109).
- Hedrick BP, Gao C, Omar GI, Zhang F, Shen C, Dodson P. 2014.** The osteology and taphonomy of a *Psittacosaurus* bonebed assemblage of the Yixian Formation (Lower Cretaceous), Liaoning, China. *Cretaceous Research* **51**(12):321–340 DOI [10.1016/j.cretres.2014.06.015](https://doi.org/10.1016/j.cretres.2014.06.015).
- Hedrick BP, Gao C, Tumarkin-Deratzian AR, Shen C, Holloway JL, Zhang F, Hankenson KD, Liu S, Anné J, Dodson P. 2016.** An injured *Psittacosaurus* (Dinosauria: Ceratopsia) from the Yixian Formation (Liaoning, China): implications for *Psittacosaurus* biology. *The Anatomical Record* **299**(7):897–906 DOI [10.1002/ar.23363](https://doi.org/10.1002/ar.23363).
- Hedrick BP, Goldsmith E, Rivera-Sylva H, Fiorillo AR, Tumarkin-Deratzian AR, Dodson P. 2020.** Filling in gaps in the ceratopsid histologic database: histology of two basal centrosaurines

- and an assessment of the utility of rib histology in the Ceratopsidae. *The Anatomical Record* **303**(4):935–948 DOI [10.1002/ar.24099](https://doi.org/10.1002/ar.24099).
- Horner JR, De Ricqlès A, Padian K. 2000.** Long bone histology of the hadrosaurid dinosaur *Maiasaura peeblesorum*: growth dynamics and physiology based on an ontogenetic series of skeletal elements. *Journal of Vertebrate Paleontology* **20**:115–129 DOI [10.1671/0272-4634\(2000\)020](https://doi.org/10.1671/0272-4634(2000)020).
- Horner JR, Goodwin MB. 2009.** Extreme cranial ontogeny in the Upper Cretaceous dinosaur *Pachycephalosaurus*. *PLOS ONE* **4**(10):e7626 DOI [10.1371/journal.pone.0007626](https://doi.org/10.1371/journal.pone.0007626).
- Horner JR, Lamm E-T. 2011.** Ontogeny of the parietal frill of *Triceratops*: a preliminary histological analysis. *Comptes Rendus Palevol* **10**(5–6):439–452 DOI [10.1016/j.crpv.2011.04.006](https://doi.org/10.1016/j.crpv.2011.04.006).
- Horner JR, Padian K. 2004.** Age and growth dynamics of *Tyrannosaurus rex*. *Proceedings of the Royal Society of London, Series B: Biological Sciences* **271**(1551):1875–1880 DOI [10.1098/rspb.2004.2829](https://doi.org/10.1098/rspb.2004.2829).
- Horner JR, ricqlès AD, Padian K, Scheetz RD. 2009.** Comparative long bone histology and growth of the Hypsilophodontid dinosaurs *Orodromeus makelai*, *Dryosaurus altus*, and *Tenontosaurus tilletii* (Ornithischia: Euornithopoda). *Journal of Vertebrate Paleontology* **29**(3):734–747 DOI [10.1671/039.029.0312](https://doi.org/10.1671/039.029.0312).
- Hu J, Forster CA, Xu X, Zhao Q, He Y, Han F. 2022.** Computed tomographic analysis of the dental system of three Jurassic ceratopsians and implications for the evolution of tooth replacement pattern and diet in early-diverging ceratopsians. *Elife* **11**:e76676 DOI [10.7554/eLife.76676](https://doi.org/10.7554/eLife.76676).
- Hübner TR. 2012.** Bone histology in *Dysalotosaurus lettowvorbecki* (Ornithischia: Iguanodontia)-variation, growth, and implications. *PLOS ONE* **7**(1):e29958 DOI [10.1371/journal.pone.0029958](https://doi.org/10.1371/journal.pone.0029958).
- Ke Y-Z, Wu R, Zelenitsky DK, Brinkman D, Hu J-F, Zhang S-K, Jiang H-S, Han F-L. 2021.** A large and unusually thick-shelled turtle egg with embryonic remains from the Upper Cretaceous of China. *Proceedings of the Royal Society B: Biological Sciences* **288**(1957):20211239 DOI [10.1098/rspb.2021.1239](https://doi.org/10.1098/rspb.2021.1239).
- Klein N, Sander PM. 2007.** Bone histology and growth of the prosauropod dinosaur *Plateosaurus engelhardti* von Meyer, 1837 from the norian bonebeds of Trosoingen (Germany) and Frick (Switzerland). *Special Papers in Palaeontology* **77**:169–206.
- Klein N, Sander M. 2008.** Ontogenetic stages in the long bone histology of sauropod dinosaurs. *Paleobiology* **34**:247–263 DOI [10.1666/0094-8373\(2008\)034](https://doi.org/10.1666/0094-8373(2008)034).
- Klein N, Sander PM, Stein K, Le Loeuff J, Carballido JL, Buffetaut E. 2012.** Modified laminar bone in *Ampelosaurus ataxis* and other titanosaurs (Sauropoda): implications for life history and physiology. *PLOS ONE* **7**(5):e36907 DOI [10.1371/journal.pone.0036907](https://doi.org/10.1371/journal.pone.0036907).
- Knoll F, Padian K, de Ricqlès A. 2010.** Ontogenetic change and adult body size of the early ornithischian dinosaur *Lesothosaurus diagnosticus*: implications for basal ornithischian taxonomy. *Gondwana Research* **17**(1):171–179 DOI [10.1016/j.gr.2009.03.010](https://doi.org/10.1016/j.gr.2009.03.010).
- Köhler M, Moyà-Solà S. 2009.** Physiological and life history strategies of a fossil large mammal in a resource-limited environment. *Proceedings of the National Academy of Sciences of the United States of America* **106**(48):20354–20358 DOI [10.1073/pnas.0813385106](https://doi.org/10.1073/pnas.0813385106).
- Lee AH, O'Connor PM. 2013.** Bone histology confirms determinate growth and small body size in the noasaurid theropod *Masiakasaurus knopfleri*. *Journal of Vertebrate Paleontology* **33**(4):865–876 DOI [10.1080/02724634.2013.743898](https://doi.org/10.1080/02724634.2013.743898).
- Lee Y-N, Ryan MJ, Kobayashi Y. 2011.** The first ceratopsian dinosaur from South Korea. *Naturwissenschaften* **98**(1):39–49 DOI [10.1007/s00114-010-0739-y](https://doi.org/10.1007/s00114-010-0739-y).

- Lee AH, Werning S. 2008.** Sexual maturity in growing dinosaurs does not fit reptilian growth models. *Proceedings of the National Academy of Sciences of the United States of America* **105**(2):582–587 DOI [10.1073/pnas.0708903105](https://doi.org/10.1073/pnas.0708903105).
- Levitt CG. 2013.** Bone histology and growth of chasmosaurine ceratopsid dinosaurs from the Late Campanian Kaiparowits Formation, southern Utah. Master Geology. The University of Utah.
- Morschhauser EM, Li D, You H, Dodson P. 2018a.** Cranial anatomy of the basal neoceratopsian *Auroraceratops rugosus* (Ornithischia: Ceratopsia) from the Yujingzi Basin, Gansu Province, China. *Journal of Vertebrate Paleontology* **38**(sup1):36–68 DOI [10.1080/02724634.2017.1399136](https://doi.org/10.1080/02724634.2017.1399136).
- Morschhauser EM, You H, Li D, Dodson P. 2018b.** Phylogenetic history of *Auroraceratops rugosus* (Ceratopsia: Ornithischia) from the Lower Cretaceous of Gansu Province, China. *Journal of Vertebrate Paleontology* **38**(sup1):117–147 DOI [10.1080/02724634.2018.1509866](https://doi.org/10.1080/02724634.2018.1509866).
- Morschhauser EM, You H, Li D, Dodson P. 2018c.** Postcranial morphology of the basal neoceratopsian (Ornithischia: Ceratopsia) *Auroraceratops rugosus* from the Early Cretaceous (Aptian-Albian) of northwestern Gansu Province, China. *Journal of Vertebrate Paleontology* **38**(sup1):75–116 DOI [10.1080/02724634.2018.1524383](https://doi.org/10.1080/02724634.2018.1524383).
- Ponce DA, Desojo JB, Cerda IA. 2023.** Palaeobiological inferences of the aetosaur *Aetosauroides scagliai* (Archosauria: Pseudosuchia) based on microstructural analyses of its appendicular bones. *Historical Biology* **35**(3):303–314 DOI [10.1080/08912963.2022.2035728](https://doi.org/10.1080/08912963.2022.2035728).
- Rainwater TR, Woodward HN, Woodward AR, Wilkinson PM. 2022.** Evidence of determinate growth in an American alligator (*Alligator mississippiensis*) based on long-term recapture and osteohistological confirmation. *The Anatomical Record* **305**(10):3101–3108 DOI [10.1002/ar.24688](https://doi.org/10.1002/ar.24688).
- Reizner JA. 2010.** *An ontogenetic series and population histology of the ceratopsid dinosaur Einiosaurus Procurvicornis* Master. Bozeman, US: Montana State University.
- Sanchez S, Steyer JS, Schoch RR, De Ricqlès A. 2010.** Palaeoecological and palaeoenvironmental influences revealed by long-bone palaeohistology: the example of the Permian branchiosaurid *Apateon*. *Geological Society, London, Special Publications* **339**(1):139–149 DOI [10.1144/sp339.12](https://doi.org/10.1144/sp339.12).
- Sander PM, Klein N, Buffetaut E, Cuny G, Suteethorn V, Le Loeuff J. 2004.** Adaptive radiation in sauropod dinosaurs: bone histology indicates rapid evolution of giant body size through acceleration. *Organisms Diversity & Evolution* **4**(3):165–173 DOI [10.1016/j.ode.2003.12.002](https://doi.org/10.1016/j.ode.2003.12.002).
- Sander PM, Klein N, Stein K, Wings O. 2011.** Sauropod bone histology and its implications for sauropod biology. In: Klein N, Remes KCG, Sander PM, eds. *Biology of the Sauropod Dinosaurs: Understanding the Life of Giants*. Bloomington and Indianapolis: Indiana University Press, 276–302.
- Sander PM, Mateus O, Laven T, Knotschke N. 2006.** Bone histology indicates insular dwarfism in a new Late Jurassic sauropod dinosaur. *Nature* **441**(7094):739–741 DOI [10.1038/Nature04633](https://doi.org/10.1038/Nature04633).
- Skutschas P, Morozov S, Averianov A, Leshchinskiy S, Ivantsov S, Fayngerts A. 2021.** Femoral histology and growth patterns of the ceratopsian dinosaur *Psittacosaurus sibiricus* from the Early Cretaceous of Western Siberia. *Acta Palaeontologica Polonica* **66**:437–447 DOI [10.4202/app.00819.2020](https://doi.org/10.4202/app.00819.2020).
- Varricchio DJ. 1993.** Bone microstructure of the Upper Cretaceous theropod dinosaur *Troodon formosus*. *Journal of Vertebrate Paleontology* **13**(1):99–104 DOI [10.1080/02724634.1993.10011490](https://doi.org/10.1080/02724634.1993.10011490).

- Waskow K, Mateus O. 2017.** Dorsal rib histology of dinosaurs and a crocodylomorph from western Portugal: Skeletochronological implications on age determination and life history traits. *Comptes Rendus Palevol* **16**(4):425–439 DOI [10.1016/j.crpv.2017.01.003](https://doi.org/10.1016/j.crpv.2017.01.003).
- Waskow K, Sander PM. 2014.** Growth record and histological variation in the dorsal ribs of *Camarasaurus* sp. (Sauropoda). *Journal of Vertebrate Paleontology* **34**(4):852–869 DOI [10.1080/02724634.2014.840645](https://doi.org/10.1080/02724634.2014.840645).
- Wells JW. 1963.** Coral growth and geochronometry. *Nature* **197**(4871):948–950 DOI [10.1038/197948a0](https://doi.org/10.1038/197948a0).
- Woodward HN, Fowler EAF, Farlow JO, Horner JR. 2015.** *Maiasaura*, a model organism for extinct vertebrate population biology: a large sample statistical assessment of growth dynamics and survivorship. *Paleobiology* **41**(4):503–527 DOI [10.1017/pab.2015.19](https://doi.org/10.1017/pab.2015.19).
- Woodward HN, Horner JR, Farlow JO. 2011.** Osteohistological evidence for determinate growth in the American alligator. *Journal of Herpetology* **45**(3):339–342 DOI [10.1670/10-274.1](https://doi.org/10.1670/10-274.1).
- Wosik M, Evans DC. 2022.** Osteohistological and taphonomic life-history assessment of *Edmontosaurus annectens* (Ornithischia: Hadrosauridae) from the Late Cretaceous (Maastrichtian) Ruth Mason dinosaur quarry, South Dakota, United States, with implication for ontogenetic segregation between juvenile and adult hadrosaurids. *Journal of Anatomy* **241**(2):272–296 DOI [10.1111/joa.13679](https://doi.org/10.1111/joa.13679).
- Xu X, Forster CA, Clark JM, Mo J. 2006.** A basal ceratopsian with transitional features from the Late Jurassic of northwestern China. *Proceedings of the Royal Society B: Biological Sciences* **273**(1598):2135–2140 DOI [10.1098/rspb.2006.3566](https://doi.org/10.1098/rspb.2006.3566).
- Xu X, Makovicky PJ, Wang X-L, Norell MA, You H-L. 2002.** A ceratopsian dinosaur from China and the early evolution of Ceratopsia. *Nature* **416**(6878):314–317 DOI [10.1038/416314a](https://doi.org/10.1038/416314a).
- You H-L, Dodson P. 2003.** Redescription of neoceratopsian dinosaur *Archaeoceratops* and early evolution of Neoceratopsia. *Acta Palaeontologica Polonica* **48**:261–272.
- You H-L, Dodson P. 2004.** Basal ceratopsia. In: *The Dinosauria (Second Edition)*. Berkeley: University of California Press, 478–493.
- You H-L, Li D-Q, Ji Q, Lamanna MC, Dodson P. 2005.** On a new genus of basal neoceratopsian dinosaur from the Early Cretaceous of Gansu Province, China. *Acta Geologica Sinica* **79**:593–597.
- Yu C-Y, Prieto-Marquez A, Chinzorig T, Badamkhatan Z, Norell M. 2020.** A neoceratopsian dinosaur from the early Cretaceous of Mongolia and the early evolution of ceratopsia. *Communications Biology* **3**(1):499 DOI [10.1038/s42003-020-01222-7](https://doi.org/10.1038/s42003-020-01222-7).
- Zhao Q, Benton MJ, Hayashi S, Xu X. 2019.** Ontogenetic stages of ceratopsian dinosaur *Psittacosaurus* in bone histology. *Acta Palaeontologica Polonica* **64**:323–334 DOI [10.4202/app.00559.2018](https://doi.org/10.4202/app.00559.2018).
- Zhao Q, Benton MJ, Sullivan C, Sander PM, Xu X. 2013.** Histology and postural change during the growth of the ceratopsian dinosaur *Psittacosaurus lujiatunensis*. *Nature Communications* **4**(1):2079 DOI [10.1038/ncomms3079](https://doi.org/10.1038/ncomms3079).
- Zhao Q, Benton MJ, Xu X, Sander PM. 2014.** Juvenile-only clusters and behaviour of the Early Cretaceous dinosaur *Psittacosaurus*. *Acta Palaeontologica Polonica* **59**:827–833 DOI [10.4202/app.2012.0128](https://doi.org/10.4202/app.2012.0128).
- Zullinger EM, Ricklefs RE, Redford KH, Mace GM. 1984.** Fitting sigmoidal equations to mammalian growth curves. *Journal of Mammalogy* **65**(4):607–636 DOI [10.2307/1380844](https://doi.org/10.2307/1380844).